Bioactive Materials 35 (2024) 477–494

Contents lists available at ScienceDirect

Bioactive Materials

journal homepage: www.keaipublishing.com/en/journals/bioactive-materials

# Urchin-like multiscale structured fluorinated hydroxyapatite as versatile filler for caries restoration dental resin composites

Shuning Zhang [a,1], Xiao Wang [a,1], Shi Yin [a], Junjun Wang [b], Hongyan Chen [a,**], Xinquan Jiang [a,*]

[a] Department of Prosthodontics, Shanghai Ninth People's Hospital, Shanghai Jiao Tong University School of Medicine, College of Stomatology, Shanghai Jiao Tong University, Shanghai Engineering Research Center of Advanced Dental Technology and Materials, National Center for Stomatology, National Clinical Research Center for Oral Diseases, Shanghai Key Laboratory of Stomatology, Shanghai Research Institute of Stomatology, No. 639 Zhizaoju Road, Shanghai, 200011, China
[b] State Key Laboratory for Modification of Chemical Fibers and Polymer Materials, College of Material Science and Engineering, Donghua University, Shanghai, 201620, China

ARTICLE INFO

*Keywords:*
Dental resin composites
Anti-caries bioactivity
Versatile fluorinated hydroxyapatite
Micromechanical interlocking
Tooth remineralization

ABSTRACT

Caries is one of the most prevalent human diseases, resulting from demineralization of tooth hard tissue caused by acids produced from bacteria, and can progress to pulpal inflammation. Filling restoration with dental resin composites (DRCs) is currently the most common treatment for caries. However, existing DRCs suffer from low fracture strength and lack comprehensive anti-caries bioactivity including remineralization, pulp protection, and anti-cariogenic bacteria effects. In this study, inspired by plant roots' ability to stabilize and improve soil, fluorinated urchin-like hydroxyapatite (FUHA) with a three-dimensional whisker structure and bioactive components of calcium, phosphorus, and fluorine was designed and synthesized by a dynamic self-assembly method. Furthermore, versatile FUHA particles with different loading fractions were used as functional fillers to fabricate methacrylate-based DRCs, where the urchin-like hydroxyapatite (UHA) filled DRCs and commercial DRCs (Z350XT and BEAUTIFIL II) served as the control groups. The results demonstrated that FUHA with 50 wt% loading in resin matrix endowed DRC (F5) with excellent physicochemical properties, dentin remineralization property, cell viability, promotion of dental pulp stem cells mineralization, and antibacterial properties. Meanwhile, F5 also presented good clinical handling and aesthetic characteristics. Therefore, structure/functional-integrated FUHA filled DRCs have potential as a promising strategy for tooth restoration and anti-caries bioactivity.

## 1. Introduction

Dental caries is one of the most prevalent oral diseases, affecting 60–90% of children and the majority of adults [1]. It is primarily caused by bacteria that metabolize sugars, producing acids which then dissolve the hard tissues of the tooth [2,3]. When the demineralization extends to the dentin, the dentin tubules are exposed, serving as gateways for caries to progress to pulpitis or even more serious diseases [4]. Especially for deep caries that progress to the inner pulpal third or quarter of dentine, there is a risk of pulp exposure [5]. Meanwhile, odontoblast layer cells and dental pulp stem cells (DPSCs) in the pulp tissue can respond to carious stimulation by synthesizing tertiary dentin, thereby forming a barrier that maintains pulp vitality. However, their natural capacity for pulp protection is limited [6,7]. Consequently, tooth cavities restorative materials which can combat the caries process effectively should be designed [5]. Dental resin composites (DRCs) are increasingly preferred for dental restorations, primarily due to their exceptional operability and aesthetic qualities [8]. However, current DRCs face challenges such as low fracture strength and insufficient therapeutic activity [9,10]. Therefore, beyond maintaining their advantages and satisfying physicochemical properties such as mechanical strength, it is essential for DRCs to possess remineralization, pulp protection, and antibacterial properties for better clinical applications.

DRCs primarily consist of fillers, resin monomers, and a

Peer review under responsibility of KeAi Communications Co., Ltd.
* Corresponding author.
** Corresponding author.
*E-mail addresses:* hychen_1201@163.com (H. Chen), xinquanjiang@aliyun.com (X. Jiang).
[1] These authors contributed equally to this work.

https://doi.org/10.1016/j.bioactmat.2024.02.004
Received 23 November 2023; Received in revised form 23 January 2024; Accepted 6 February 2024

photoinitiator system [11]. The structure and composition of fillers significantly influence the filler/resin matrix interface interaction and physicochemical-biological performances, such as mechanical properties, antibacterial properties, cytological properties, etc. [12–14]. Commonly used fillers are spherical or irregularly structured, which are susceptible to detachment from the resin matrix under occlusal forces, potentially leading to fractures of the restoration materials [15]. Additionally, these fillers typically lack significant anti-caries activities and may easily contribute to the development of secondary caries and pulpitis [15].

Learning from nature, we observe that plants withstand external forces or harsh weather conditions, largely due to their unique root system comprising numerous dispersed whiskers. These roots penetrate into the soil, forming a mechanically interlocking structure that strengthens the root-soil interface [16,17]. Meanwhile, this interface is dynamic, where the root system releases carbohydrates and vitamins, influencing the soil's microbial community, physicochemical properties, and nutrient content, which in turn affect the growth and health of plants [18,19]. Inspired by this root system and the rhizosphere effect, fluorinated urchin-like hydroxyapatite (FUHA) with root-like structure and tooth-mimicking bioactive components (fluorinated hydroxyapatite, FHA) [20] was synthesized and then used as fillers in methacrylate-based DRCs in this study. FUHA showed a three-dimensional (3D) urchin-like structure assembled from central-radial one-dimensional (1D) nanowhiskers. Each 1D whisker in FUHA can individually play the reinforcing roles of crack deflection, whisker breakage, whisker pullout, and whisker bridging in DRCs [21,22]. Additionally, the 3D whisker structure can address the issue of 1D nanowhisker agglomeration and enhance filler/resin matrix interface interaction by micromechanical interlocking through nanobranches in various orientations [23–25]. The composition of FUHA, similar to natural teeth, offers better mechanical strength, lower solubility, and great acid and caries resistance than hydroxyapatite (HA), which are crucial for DRCs in a moist oral environment [26,27]. Furthermore, fluoride is known for its antibacterial properties [28], and FHA has been widely reported as a bioactive substance that promotes stem cell differentiation and hard tissue formation [29–31]. These properties make FHA an effect agent to resist caries microenvironment and protect pulp when used as the fillers in DRCs. However, the antibacterial activity and promotion of DPSCs' mineralization properties in FHA-filled DRCs have not been studied. In addition, to the best of our knowledge, no previous studies have reported the simultaneous integration of excellent mechanical properties, remineralization, pulp protection, and antibacterial functions in DRCs through a single filler.

Herein, inspired by the structure-function integration of plant roots, we selected FHA as a functional component and synthesized it into an urchin-like 3D whisker structure (FUHA) through a one-step hydrothermal reaction at high temperature and pressure. Furthermore, the FUHA particles underwent silanization and were employed as fillers to construct DRCs. Compared to commercial DRCs and urchin-like hydroxyapatite (UHA)-filled DRCs, the physicochemical properties and the ability to remineralize demineralized dentin of FUHA-filled DRCs were investigated by viscosity, curing, mechanics, aesthetics, water absorption, solubility, and ionic release tests, as well as models of demineralized dentin in a simulated oral environment. Meanwhile, the impacts of these DRCs on DPSCs and cariogenic bacteria were further evaluated in terms of cell activity, differentiation and mineralization, as well as bacterial adhesion and activity. FUHA has emerged as a promising filler for DRCs, demonstrating comprehensive capabilities for the treatment of cavitated caries, particularly in the management of deep caries (Scheme 1).

## 2. Materials and methods

### 2.1. Materials

Bisphenol A glycidyl methacrylate (Bis-GMA, ≥99%), triethylene glycol dimethacrylate (TEGDMA, 95%), urethane dimethacrylate (UDMA, ≥97%), ethyl 4-dimethylamino benzoate (4-EDMAB, 99%), camphorquinone (CQ, 97%), and 3-methacryloxypropyl trimethoxysilane (γ-MPS, 99%) were purchased from Sigma-Aldrich Co., Ltd. (Shanghai, China). Ethylenediaminetetraacetic acid disodium salt (EDTA·2Na), disodium hydrogen phosphate dodecahydrate ($Na_2HPO_4 \cdot 12H_2O$), and n-propylamine (99%) were purchased from Sinopharm Chemical Reagent Co., Ltd. (Shanghai, China). Calcium nitrate tetrahydrate [$Ca(NO_3)_2 \cdot 4H_2O$], sodium fluoride (NaF), sodium hydroxide (NaOH), cyclohexane (99%), hydrochloric acid (HCl, 37 wt%), and acetic acid ($CH_3COOH$, ≥99.5%) were purchased from Shanghai Lingfeng Chemical Reagent Co., Ltd. (Shanghai, China). Sodium chloride (NaCl), sodium bicarbonate ($NaHCO_3$), potassium chloride (KCl), dipotassium hydrogen phosphate trihydrate ($K_2HPO_4 \cdot 3H_2O$), magnesium chloride ($MgCl_2$), calcium chloride ($CaCl_2$), sodium sulphate ($Na_2SO_4$), phosphoric acid ($H_3PO_4$, 85%) and potassium dihydrogen phosphate ($KH_2PO_4$) were purchased from Shanghai Aladdin Bio-Chem Technology Co., Ltd. (Shanghai, China). Deionized water and phosphate buffered saline (PBS) were obtained from our own laboratory.

### 2.2. Synthesis and silanization of FUHA

The FUHA particles were prepared using a one-step hydrothermal

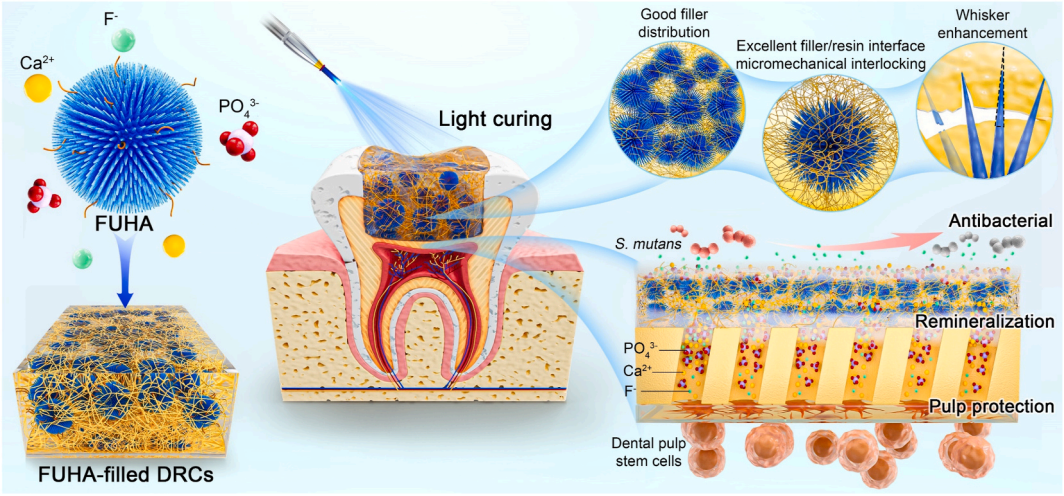


**Scheme 1.** Scheme of FUHA-filled light-curing DRCs for dentin caries restorations.

method (Fig. 1A). Briefly, EDTA·2Na (29.78 g), $Ca(NO_3)_2{\cdot}4H_2O$ (18.89 g), $Na_2HPO_4{\cdot}12H_2O$ (17.21 g), and NaF (0.34 g) were added sequentially into a beaker containing deionized water (400 mL) under stirring at room temperature, and then the pH of the above solution was adjusted to 12.5 using solid NaOH. Subsequently, this mixture was moved into a Teflon-lined autoclave and heated at 180 °C for 1 h. The FUHA powders were obtained by centrifugation, washed with water and vacuum-dried at 90 °C for 10 h. UHA particles were prepared using the same procedure, but without adding NaF.

Subsequently, FUHA (10 g) or UHA (10 g) was dispersed in cyclohexane (200 mL) with ultrasonic treatment, and then, n-propylamine (0.28 mL) and γ-MPS (1.06 g) were added under magnetic stirring for 30 min at 30 °C. The obtained mixture was further stirred for 1 h at 60 °C. The silanized FUHA or silanized UHA powders were obtained by centrifugation, washed with water and vacuum-dried at 90 °C for 12 h.

### 2.3. Fabrication of DRCs filled with FUHA

The as-prepared silanized FUHA was used as a unimodal filler to fabricate DRCs. Firstly, a resin matrix was obtained by mixing monomers (Bis-GMA/TEGDMA/UDMA, 39.6/29.7/29.7, wt/wt/wt) and a photoinitiator system (CQ/4-EDMAB, 0.2/0.8, wt/wt) at a dark environment. Then, FUHA with different mass fractions was blended with the resin matrix by a SpeedMixer (DAC 150.1 FVZ-K, Germany) and a three-roll mixer (EXAKT 80E, Germany). The composite pastes produced by these processes were placed in the dark for later use. DRCs filled with UHA were constructed using the same procedure and served as the control group. The DRCs are denoted as H3 (UHA filling: 30 wt%), H5 (UHA filling: 50 wt%), F3 (FUHA filling: 30 wt%), and F5 (FUHA filling: 50 wt%), respectively.

To the preparation of cured samples for subsequent testing, the composite pastes were inserted into the silicon rubber molds and polymerized with a light curing unit (Bluephase N MC, USA). All cured samples were polished before further experiments. The commercial DRCs Z350XT (3M, USA) was selected as a control, and BEAUTIFIL II (SHOFU, Japan) was chosen as a positive control for the antibacterial test.

### 2.4. Characterization of particles

The morphology structure of the synthetic particles (UHA and FUHA) were determined using Field Emission Scanning Electron Microscopy (FE-SEM, ZEISS Sigma 300, Germany) and Transmission Electron Microscopy (TEM, Thermo Scientific, USA) with operating voltages of 5.0 kV and 200 kV, respectively. Elemental mapping was performed by an analytical TEM equipped with an Energy Dispersive Spectrometer (EDS) system. The compositions and crystalline structures of the particles were evaluated by X-ray Photoelectron Spectroscopy (XPS, Escalab 250Xi, USA) and X-ray Diffractometry (XRD, D/Max-2550 PC, RIGAKU, Japan), respectively. The polymer grafting rates of silanized UHA and silanized FUHA were evaluated by Fourier Transform Infrared Spectroscopy (FT-IR, Nexus-670, USA) and Thermogravimetric Analysis (TGA, PerkinElmer, USA), respectively. In addition, the particles' morphology structures dissolved from each DRC paste were also be evaluated by FE-SEM, where 500 mg of each DRC paste was immersed in 5 mL of acetone to removing the resin matrix and finally obtaining the particles.

### 2.5. Physicochemical properties of DRCs

#### 2.5.1. Viscosity

The viscosity of the DRCs was determined using a rotational rheometer (HAAKE MARS 60, Germany). Each composite paste was placed between 20 mm parallel plates. Frequency test was carried out in oscillation mode at a constant strain of 0.1%. Shear viscosity (η) was measured as a function of shear frequency (0.01–10 rad/s) at 37 °C.

#### 2.5.2. Curing depth

According to ISO 4049-2019 [32], each composite paste was placed in a cylindrical mold (Φ 4 mm × 10 mm) and irradiated vertically against the paste surface on one side using a light curing unit. After 20 s, the sample was removed, and an adjusting knife was used to scrape off the softer uncured material until no more could be scraped off manually. The height of the remaining cured material was then measured with vernier caliper. The ISO-specified light-curing depth was determined by dividing the measurement by 2.

#### 2.5.3. Degree of conversion (DC)

A FT-IR spectrometer (Nicolet 8700, Germany) equipped with an Attenuated Total Reflection (ATR) crystal was used to determine DC of DRCs. Each composite paste was filled into a cylindrical silastic mold with a diameter of 4 mm and a thickness of 2 mm, then the FT-IR absorption curves at 600-4000 $cm^{-1}$ were measured before and after curing 60 s. Subsequently, the DC value of each DRC was determined from the height of the absorption band of the aliphatic C═C bond (1638 $cm^{-1}$) versus the internal standard aromatic C═C bond (1608 $cm^{-1}$) using the following Eq. (1) [33]:

$$DC\ (\%) = \left[1 - \frac{(h_{1638}/h_{1608})_{cured}}{(h_{1638}/h_{1608})_{uncured}}\right] \times 100 \quad (1)$$

where *h1638/h1608* is the ratio of the height of the absorption peak at 1638 $cm^{-1}$ to that at 1608 $cm^{-1}$.

#### 2.5.4. Mechanical properties and fracture morphology

The mechanical properties of the DRCs, including flexural strength (FS), flexural modulus (FM), work of fracture (WOF), fracture toughness ($K_{IC}$), and compressive strength (CS) were evaluated using a universal testing machine (LLOYD EZ20, USA). Each composite paste was placed into different molds for corresponding tests: a rectangular-shaped mold (25 mm × 2 mm × 2 mm) for FS, FM and WOF tests, a rectangular-shaped mold with a single-edge-V-notched beam (25 mm × 5 mm × 3 mm with a single notch of 2.5 mm depth on a 3mm × 5 mm surface) for KIC test, and a cylindrical specimen (Φ 4 mm × 6 mm) for CS test, respectively. All the cured specimens were polished with silicon carbide paper, and then measured with 0.75 mm/min loading rate according to ISO 4049-2019. The fracture morphologies of the specimens after flexural tests were analyzed by FE-SEM. The detailed equations for calculating these mechanical properties were Eqs. (2)–(7) [34–36], with Eq. (6) applied in the operation of Eq. (5):

$$FS = \frac{3Fl}{2bh^2} \quad (2)$$

$$FM = \frac{Fl^3}{4bh^3d} \quad (3)$$

$$WOF = \frac{A}{bh} \quad (4)$$

$$K_{IC} = \frac{Fl}{bh^{3/2}} f\left(\frac{a}{h}\right) \times \sqrt{10^{-3}} \quad (5)$$

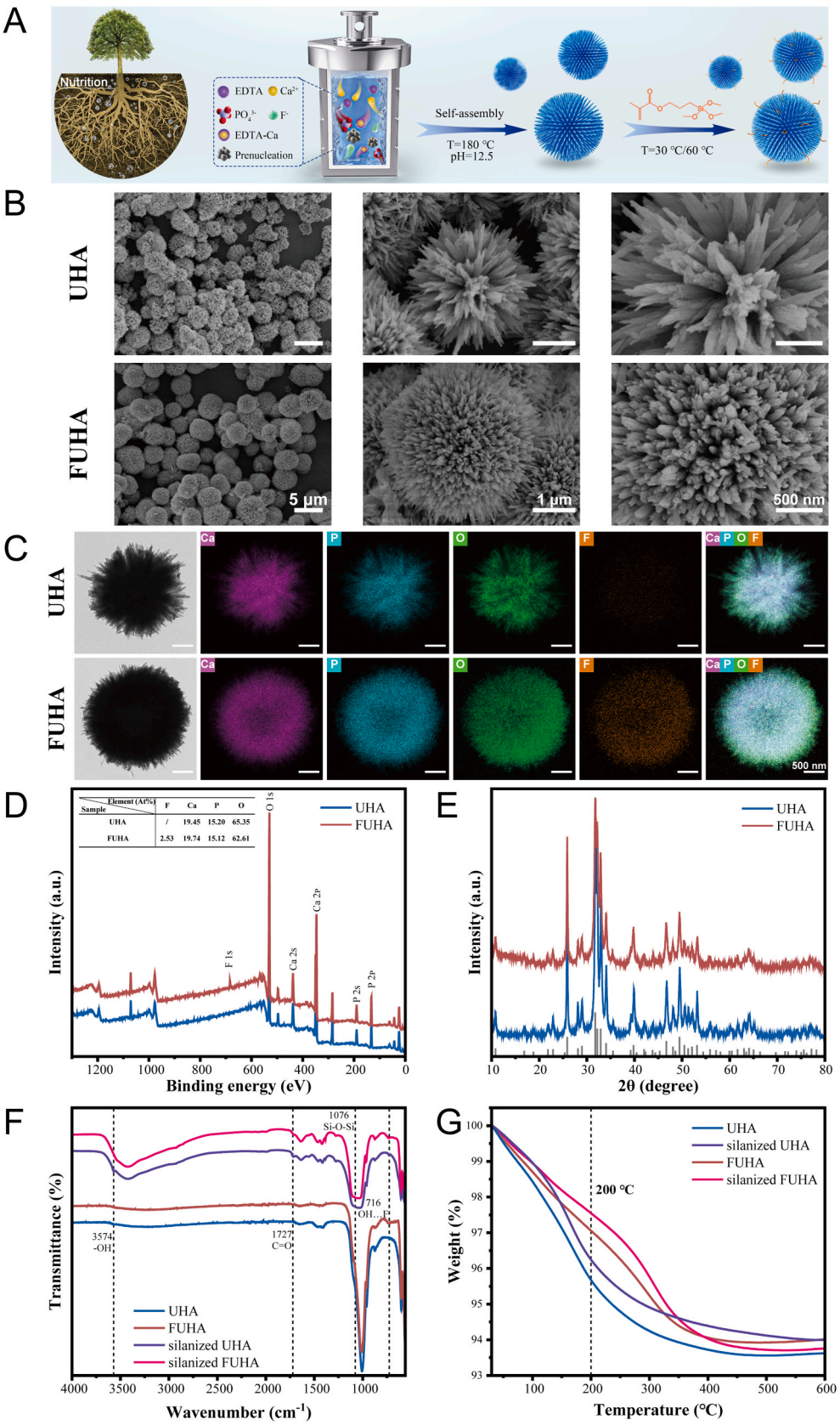


**Fig. 1.** Characterization of UHA, FUHA and their silanization. (A) Flowchart for the synthesis of root-inspired FUHA. (B) FE-SEM images of UHA and FUHA. (C) TEM images and elemental mapping of UHA and FUHA. (D) XPS spectra and contents of F, Ca. P, O in UHA and FUHA. (E) XRD patterns of UHA and FUHA, HA standard card JCPDS: 09–0432 (gray line). (F) FT-IR spectra and (G) TGA curves of UHA, FUHA, silanized UHA, and silanized FUHA.

$$f(a/h)=3(a/h)^{1/2}\left\{\frac{1.99-(a/h)(1-a/h)\left[2.15-3.93(a/h)+2.7(a/h)^2\right]}{2[1+2(a/h)](1-a/h)^{3/2}}\right\} \quad (6)$$

$$CS=\frac{4F}{\pi D^2} \quad (7)$$

where $F$ (N) is the maximum load, $l$ (mm) is the span length of the specimen, $b$ (mm) is the width of the specimen, $h$ (mm) is the height of the specimen, $d$ (mm) is the deflection under maximum load, $A$ (kJ) is the area under the load-displacement curve, $a$ (mm) is the pre-crack depth of the specimen, and $D$ (mm) is the diameter of the specimen.

#### 2.5.5. Light transmission

Disc specimens (Φ 15 mm × 1 mm) of each DRC were prepared and their transmittance in the wavelength range of 200–800 nm was recorded using an ultraviolet–visible–near-infrared (UV–vis–NIR) spectrophotometer (PerkinElmer Lamada 950, USA). The images of the specimens covered with the blue emblem of Shanghai Jiao Tong University were also recorded by a digital camera (Canon EOS 200D II, Japan).

#### 2.5.6. Release behavior of $Ca^{2+}$, $PO_4^{3-}$, and $F^-$ in liquid

Each category of cured DRCs samples, consisting of nine discs (Φ 10 mm × 1 mm), was divided into three distinct groups (n = 3), and then each disc was individually immersed in 12 mL of deionized water for different time points (7, 14, and 30 days) at 37 °C. At each time point, the solutions were collected. The concentration of $Ca^{2+}$ was analyzed by Inductively Coupled Plasma Optical Emission Spectrometer (ICP-OES, Shimadzu ICPE-9800, Japan), and the concentrations of $PO_4^{3-}$ and $F^-$ were analyzed by Ion Chromatography (IC, Thermo Scientific ICS-5000+, USA). Additionally, the ions release of DRCs in simulated body fluid (SBF, Table S1) [37] for 7 and 30 days were also evaluated using the same methods.

#### 2.5.7. Water absorption and solubility

According to ISO 4049-2019, various DRCs specimens (Φ 15 mm × 1 mm) were placed in a drying oven at 37 °C for 22 h and then their weights were recorded. The procedure was repeated until a constant mass ($m_1$) was obtained. The average diameter and thickness of each specimen were determined with a vernier caliper to an accuracy of ±0.01 mm and the volume was calculated. All specimens were then immersed in deionized water and placed at 37 °C. At different time points (1, 7, 14, and 30 days), three specimens of each DRC were taken out, dried on filter paper, and weighed to obtain the mass ($m_2$). The above drying process was repeated until a constant mass ($m_3$) was obtained. The water absorption ($W_{sp}$) and solubility ($W_{sl}$) of the DRCs were calculated using the following Eq. (8) and Eq. (9) [32]:

$$W_{sp}=\frac{m_2-m_3}{V} \quad (8)$$

$$W_{sl}=\frac{m_1-m_3}{V} \quad (9)$$

where $m_1$ (μg) is the mass of the specimen before immersion in water, $m_2$ (μg) is the mass of the specimen after immersion in water for different times, $m_3$ (μg) is the mass of the specimen after re-drying, and $V$ is the volume of the specimen ($mm^3$).

#### 2.5.8. Mechanical stability

To evaluate the mechanical stability of DRCs, the cured specimens (25 mm × 2 mm × 2 mm) were immersed in the SBF (pH = 7.4 or pH = 4.0 using HCl to adjust) for 14 and 30 days. After that, the FM and FS were measured using the universal testing machine.

### 2.6. Remineralization properties

#### 2.6.1. Mineralization of DRCs surfaces

Based on the above physicochemical properties of DRCs, F5 was selected as the representative material to evaluate remineralization properties, with H5 and Z350XT serving as the control groups. Various cured specimens (Φ10 mm × 1 mm) were immersed in 15 mL of SBF (pH = 7.4) at 37 °C for 1, 14, and 30 days to assess their surface mineral deposition. Additional, to evaluate mineralization deposition in an acidic milieu, the solution was changed to pH = 4 and the specimens were immersed for 30 days. At each time point, the specimens were carefully extracted, gently rinsed with deionized water, and subsequently dried in a dying oven set at 40 °C for 24 h. Post-drying, the formation of the mineralized layer on the surfaces of the samples was examined using FE-SEM.

#### 2.6.2. Remineralization of DRCs for demineralized dentin

To assess the remineralization property of DRCs on dentin, demineralized dentin samples were prepared. Caries-free posterior teeth were collected following informed consent from the patients and with the approval of the Ethics Committee of the Ninth People's Hospital Affiliated to Shanghai Jiaotong University School of Medicine (SH9H-2020-T298-3). 1-mm-thick dentin slices were obtained by cutting dentin samples at 2 mm above the cemento-enamel junction using a cutting machine (Mecatome T210, France), where one slice obtained from each tooth. Then, the dentin slices were acid-etched using 37% $H_3PO_4$, and placed on a shaker for 15 s, followed by gently rinsing with deionized water for 30 s and gentle blowing for 20 s to form demineralized dentin slices [38]. Subsequently, 1-mm-thick layers of Z350XT, H5, and F5 were coated on the demineralized dentin slices and light-cured for 30 s. The dentin slices without acid-etching and those acid-etched without DRCs treatment were set as control groups. After that, the samples were soaked in 5 mL of SBF (pH = 7.4) at 37 °C for 14 days, with the solution changed every other day. Finally, after fixation with 2.5% glutaraldehyde and dehydration with gradient ethanol, mineral formation and the elemental composition on the surface of the dentin slices were observed using FE-SEM and corresponding element mapping. Additionally, the dentin slices were delicately bisected for examination of remineralization within the dentin tubules. Moreover, the microhardness of the various slices was measured using a Vickers hardness tester (HX-1000TM/LCD, China) by applying a load of 50 gf for 15 s.

#### 2.6.3. Micro computed tomography (Micro-CT) analysis of dentin remineralization

In order to quantify the remineralization effect of different DRCs, chemical caries models were also prepared. Firstly, cavities (Φ1 mm × 1 mm) were prepared using a dental high-speed handpiece (Pana·Max2 M4, Japan) on 2-mm-thick dentin slices. Then, the surface of the above dentin was coated with acid-resistant nail polish (OPI, USA) except for the cavities, and artificial dentin caries samples were fabricated by immersing the samples in a solution containing 3 mM $Ca^{2+}$ and 3 mM $H_2PO_4^-$ as well as 50 mM $CH_3COOH$ at pH = 5.0 for 14 days [39].

The chemical caries was observed using Micro-CT (SkyScan 1076 X-ray microtomography system, Belgium; Scanning parameters: 70 kV, 141 μA, 1850 ms, 0.6° per rotation) to confirm the demineralization

formation. Subsequently, the caries cavities were respectively filled with Z350XT, H5, and F5, followed by light-curing. Then, all samples were placed in 10 mL of SBF (pH = 7.4) at 37 °C, with the solution changed every other day. After 30 days, the chemical caries was evaluated by Micro-CT again. Finally, the densities of the formerly acid-etched areas treated with different DRCs were calculated.

### 2.7. In vitro cell activity

#### 2.7.1. Human dental pulp stem cells (hDPSCs) culture

Healthy teeth were collected from Shanghai Ninth People's Hospital affiliated with Shanghai Jiaotong University School of Medicine after informed consent. Firstly, the teeth were dissected to expose the pulp tissues in a sterile environment. The pulp tissue was then separated, cut into small pieces and pressed with a coverslip in a Petri dish. Subsequently, cell culture medium containing Dulbecco's Modified Eagle's Media (DMEM, Hyclone, USA), 10% fetal bovine serum (FBS, Gibco, USA), and 1% penicillin/streptomycin (Gibco, USA) was added into the above dish and placed at 37 °C under a 5% $CO_2$ atmosphere. Finally, the hDPSCs crawled out of the tissue block, and the cells of generation 3–6 were used in this study [40].

#### 2.7.2. Preparation of specimen extracts

DRCs disc pieces (Φ 10 mm × 1 mm) were prepared, sterilized by UV irradiation for 30 min on each side, and washed three times with PBS. Subsequently, these discs were immersed in DMEM (containing 10 % FBS and 1% penicillin/streptomycin) or in osteogenic induction medium (OriCell®, China). Specimen extracts were obtained after incubation at 37 °C for 72 h. The ratio of the volume of culture medium to the surface area of the specimen was 3 $cm^2$/mL, according to the ISO-10993 standard [41].

#### 2.7.3. Cytotoxicity and cell proliferation

The hDPSCs were seeded in 48-well plates ($10^4$ cells/well) and cultured with DRCs extract. After 1, 4, and 7 days, the Calcein-AM/PI Double Stain Kit (Yeasen, China) was used to conduct the Live/Dead assay, and the cells morphology was observed using a fluorescence microscope (Olympus, Japan). The surface coverage of the different fluorescence was analyzed by ImageJ software (Rawak Software, Germany). Additionally, hDPSCs were seeded in 96-well plates ($4 \times 10^3$ cells/well) and the Cell Counting Kit-8 (CCK-8, Yeasen, China) tests were performed at 1, 3, 5, and 7 days, where the optical density (OD) of solution at λ = 450 nm was measured using an enzyme labeling instrument (TECAN Spark, Switzerland).

#### 2.7.4. Cell migration

The hDPSCs migration was measured by a transwell-migration assay. In brief, 0.6 mL of each DRCs extract (DMEM without FBS) was added to the transwell insert's lower chamber, and the hDPSCs were cultured on the transwell insert's upper chamber in 0.2 mL of DMEM for 24 h. Next, the transwell chambers were fixed in 4% paraformaldehyde (Beyotime, China) for 15 min and stained with 0.5% crystal violet (Beyotime, China) for 15 min. Subsequently, the hDPSCs that did not penetrate the filter were wiped away with cotton swabs, and the cells that migrated to the undersurface of the filter were observed by a microscope (Olympus, Japan) and analyzed by ImageJ software.

### 2.8. In vitro mineralization of hDPSCs

#### 2.8.1. Alkaline phosphatase (ALP) activity test

The hDPSCs were cultured with osteogenic induction medium extracts of DRCs for 14 days, and a blank control was set. For ALP staining, the cells were fixed with 4% paraformaldehyde for 30 min. Subsequently, the fixative was removed and the cells were stained using BCIP/NBT Alkaline Phosphatase Chromogenic Kit (Beyotime, China). The staining images were observed by an inverted microscope (Nikon, Japan). For the ALP activity assay, after lysis with 1% Triton X-100 (Beyotime, China) for 30 min, the ALP protein of the hDPSCs was measured by an Alkaline Phosphatase Assay Kit (Beyotime, China) and recorded as the OD value at 405 nm. Next, the total protein concentration in each sample was determined using a BCA protein assay kit (Thermo, USA) for normalization.

#### 2.8.2. Alizarin red S (ARS) staining

After the hDPSCs were cultured with osteogenic induction medium extracts of DRCs for 21 days, ARS staining was evaluated qualitatively and quantitatively. The staining images were recorded after the cells were fixed with 4% paraformaldehyde and stained with ARS (OriCell®, China). For quantitative analysis, cells stained with ARS were eluted with 10% cetylpyridinium chloride (Macklin, China), and the OD value of the eluate was measured at 620 nm.

#### 2.8.3. Real-time polymerase chain reaction (RT-PCR) analysis

The expression of mineralization-related genes in hDPSCs was detected by RT-PCR. After incubating the hDPSCs with osteogenic induction medium extracts of DRCs for 14 days, RNA was isolated using TRIzol (Invitrogen, USA). After measuring the RNA concentration and purity with a NanoDrop™ 1000 ultraviolet–visible spectrophotometer (Thermo Scientific, USA), the RNA was converted to cDNA using a PrimeScriptTM RT kit (Takara, Japan). Subsequently, RT-PCR for ALP, osteocalcin (OCN), and osteopontin (OPN) was performed using a LightCyler 480 (Roche, Switzerland) and SYBR Green (Yeasen, China). Glyceraldehyde-3-phosphate dehydrogenase (GAPDH) was used as the housekeeping gene, and the results were quantified by the $2^{-\Delta\Delta Ct}$ method. Assays for dentin matrix protein-1 (DMP-1) and dentin sialophosphoprotein (DSPP) genes were obtained from hDPSCs conditioned cultured for 21 days in the same way as described above. The forward and reverse primers (Shenggong Co., Ltd. Shanghai, China) used in this study were listed in Table S2.

#### 2.8.4. Immunofluorescence staining

The expression of OCN and OPN in hDPSCs after culturing with DRCs osteogenic induction extracts for 14 days was examined by immunofluorescence staining. In brief, hDPSCs were fixed with 4% paraformaldehyde for 20 min and permeabilized with 0.1% Triton X-100 for 30 min, then they were incubated with OCN (Abclonal, USA) and OPN (Proteintech, USA) primary antibodies at 4 °C overnight. After that, the cells were incubated with DyLight 488-conjugated Goat Anti-Rabbit IgG (Abclonal, USA) for 1 h at room temperature, and the cytoskeleton was stained with Rhodamine Phalloidin (Abclonal, USA) for 1 h, the nuclei were stained with DAPI (Beyotime, China) for 5 min. Afterwards, the results were observed under a fluorescence microscopy.

### 2.9. Antibacterial analysis

#### 2.9.1. Bacterial spread plate test

*Streptococcus mutans* (*S. mutans*, UA159) was obtained from the Ninth People's Hospital of Shanghai Jiao Tong University School of Medicine and cultured with Brain Heart Infusion (BHI, Solarbio, China) broth at 37 °C in anaerobic chamber. The solid medium for *S. mutans* was BHI that containing 2% agarose (Solarbio, China).

Firstly, the cured specimens (Φ 10 mm × 1 mm) of Z350XT, BEAUTIFIL II, H5, and F5 were polished and sterilized by UV irradiation. 800 μL of a bacterial suspension ($1 \times 10^6$ CFU/mL) was co-incubated with each specimen at 37 °C for 24 h in an anaerobic chamber. Subsequently, the bacterial solution was removed and the different specimens were rinsed with PBS to remove unattached bacteria. Next, the specimens were placed in 8 mL of sterile PBS and ultrasonicated for 5 min to detach the bacteria that adhering on the sample surface. Afterwards, 50 μL of the bacterial suspension was spread on agar plates after $10^4$-fold dilution. Finally, the plates were incubated at 37 °C for 48 h and the number of colony forming unit (CFU) on the plates was recorded. The

antibacterial rate was calculated using the following Eq. (10) [42]:

$$C\ (\%) = \frac{A - B}{A} \times 100 \quad (10)$$

where $C$ is the antibacterial rate, $A$ is the average CFU of the control group (Z350XT), and B is the average CFU of the experimental groups (BEAUTIFIL II, H5, and F5).

#### 2.9.2. Live/dead bacterial staining

A bacterial suspension ($1 \times 10^6$ CFU/mL, 800 μL) was co-cultured with each cured specimen at 37 °C for 72 h in an anaerobic chamber. Subsequently, 200 μL of the above bacterial solution was stained using the Live/Dead Bacteria Dual Staining Kit (Bestbio, China). Images and numbers of live/dead bacteria were obtained using a fluorescence microscope and ImageJ software, respectively.

#### 2.9.3. Acid neutralization of DRCs

Cured specimens (Φ15 mm × 1 mm) of DRCs were submerged in SBF (10 mL, pH = 4) and stored at 37 °C in a dark environment. The pH value of the SBF was measured using a Meter FP20-Std-Kit (METTLER TOLEDO, Switzerland) at days of 1, 7, 14, and 21, respectively.

#### 2.9.4. Wear resistance of DRCs

The cured specimens (Φ10 mm × 1 mm) were polished with P3000 Silicon Carbide (SiC) paper for 20 s using a polishing machine (Beta, USA) under water cooling conditions. The surface roughness (Ra) of the polished specimens was determined by Perthometer M1 (Mahr, Germany) (Lt = 5.6 mm, λc = 0.800 mm).

### 2.10. In vivo study

*In vivo* animal study was performed with the approval of the Ethics Committee of the Ninth People's Hospital Affiliated to Shanghai Jiao Tong University School of Medicine (SH9H-2023-A794). Male Sprague-Dawley rats (8 weeks old, 250–300 g, n = 3) were anesthetized with 1% pentobarbital sodium (0.4 mL/100 g) via intraperitoneal injection. Following the method described in section 2.6.2, six 1-mm-thick human dentin slices were prepared, and two holes were punched in each slice for fixation in the rat's oral cavity. All dentin slices were etched using the method in 2.6.2 and assigned to two treatment groups (Z350XT group and F5 group). The acid-etched dentin slices were fixed on the buccal mucosa of the rat oral cavity (Fig. 8A). Dentin slices were sewn on both sides, with 1-mm-thick Z350XT paste applied to the dentin slice on one side, and 1-mm-thick F5 paste was applied to the other side, followed by light curing for 1 min. The rats were fed a cariogenic Keyes 2000 diet (obtained from Nantong Trophy Feed Technology Co., Ltd.) and 5% sucrose-containing water, and the surfaces of the materials were coated with *S. mutans* ($10^7$ CFU/mL, 200 μL) every other day to establish a cariogenic environment during incubation. After 14 days, the dentin slices were removed, fixed with 2.5% glutaraldehyde, and dehydrated using alcohol gradients. The bacterial situations on the surfaces of the materials were checked using FE-SEM, then the DRCs on the dentin slices were removed, and the remineralization of demineralized dentin was observed using FE-SEM.

### 2.11. Statistical analysis

All results were expressed as the mean ± standard deviation (SD), which derived from a minimum of three independent experiments (n = 5 in mechanical property tests and n = 3 in other tests). One-way ANOVA with Tukey's multiple comparisons was conducted using GraphPad Prism 9 and Origin 2022 software to assess statistical significance between groups, with significance accepted at $p < 0.05$.

## 3. Results and discussion

### 3.1. Characterization of particles

Inspired by the interface interaction between plant roots and soil, UHA and FUHA particles with root-like structure were synthesized according to the nucleation-growth process at high-pH environment with EDTA chelating $Ca^{2+}$, which involved complex dynamic self-assembly [43] (Fig. 1A). As shown in SEM images, both UHA and FUHA presented urchin-like morphology, consisting of tapered nanowhiskers that extended radially from the center and were three-dimensionally distributed. And the surface of each tapered nanowhisker was rough, which could further increase its interfacial contact area when mixed with the organic phase (Fig. 1B) [44]. In addition, compared to UHA, FUHA had a more concentrated particle size distribution (3–4 μm in diameter), and the introduction of fluorine increased the density of the whiskers. An appropriate increase in whisker density could optimize the mechanical interlocking effect of the particles when embedded in the resin matrix [45]. The structure and composition of the particles were further evaluated by TEM images and corresponding elemental mapping (Fig. 1C and Fig. S1). The results showed that both UHA and FUHA contained a large amount of Ca, P, and O elements, which were uniformly distributed throughout the particles. Compared with UHA, the F element was clearly observed and distributed uniformly in FUHA particle. In addition, their elemental compositions were further characterized by XPS (Fig. 1D), which showed a significant fluorine signal (At%: 2.53%) in FUHA, indicating that fluorine was successfully introduced into the FUHA. The crystal structures of particles were evaluated by XRD, and their characteristic peaks matched those of HA (ICDD 09–0432), as illustrated in Fig. 1E. FT-IR analysis was conducted to evaluate the chemical structures of the particles, and the results were presented in Fig. 1F. Compared with UHA, the introduction of F element in FUHA weakened the absorption peak at position 3574 $cm^{-1}$ that corresponding to the –OH in the particles [46], and gave rise to a new characteristic peak at 716 $cm^{-1}$ indicative of the stretching vibration of the OH···F [47]. These results suggested that F in FUHA was the replacement of –OH on the surface of UHA. Furthermore, the presence of characteristic peaks of C═O at 1727 $cm^{-1}$ and Si–*O*–Si at 1076 $cm^{-1}$ in silanized UHA and FUHA particles indicated that γ-MPS was successfully grafted onto the surface of UHA and FUHA [48,49]. The grafting rates of γ-MPS onto particles were further quantitatively assessed by TGA measurements (Fig. 1G). The weight loss below 200 °C mainly originated from physically adsorbed water and the unreacted γ-MPS [50]. The grafting rates of γ-MPS, calculated based on the weight change from 200 °C to 600 °C, were found to be 0.20 wt% for UHA and 0.75 wt% for FUHA. The higher polymer grafts on FUHA's surface could help improve the FUHA/resin matrix interface interaction, and further optimize the mechanics properties [51].

### 3.2. Physicochemical properties of DRCs

In this study, during the constructions of DRCs filled with UHA or FUHA, the composite paste broke apart and turned into the coarse powder when the filler loading exceeded 50 wt%. Compared with the nonporous fillers used in commercial DRCs, the filler loading of UHA or FUHA was lower. This phenomenon was mainly attributed to the large specific surface area of the urchin-like structure. Consequently, the fillers could not be sufficiently infiltrated and wrapped by the organic phase when an excessive amount of fillers were added [8]. Therefore, we chose 30 wt% and 50 wt% filler loading as the experimental groups in this study.

The clinical operability of DRCs plays a pivotal role in their effectiveness for doctors and patients. A critical aspect is the viscosity of the uncured DRCs, which strongly depends on the composition and structure of the fillers and resin matrix [52]. As shown in Fig. 2A, all experimental DRCs and commercial Z350XT exhibited shear-thinning

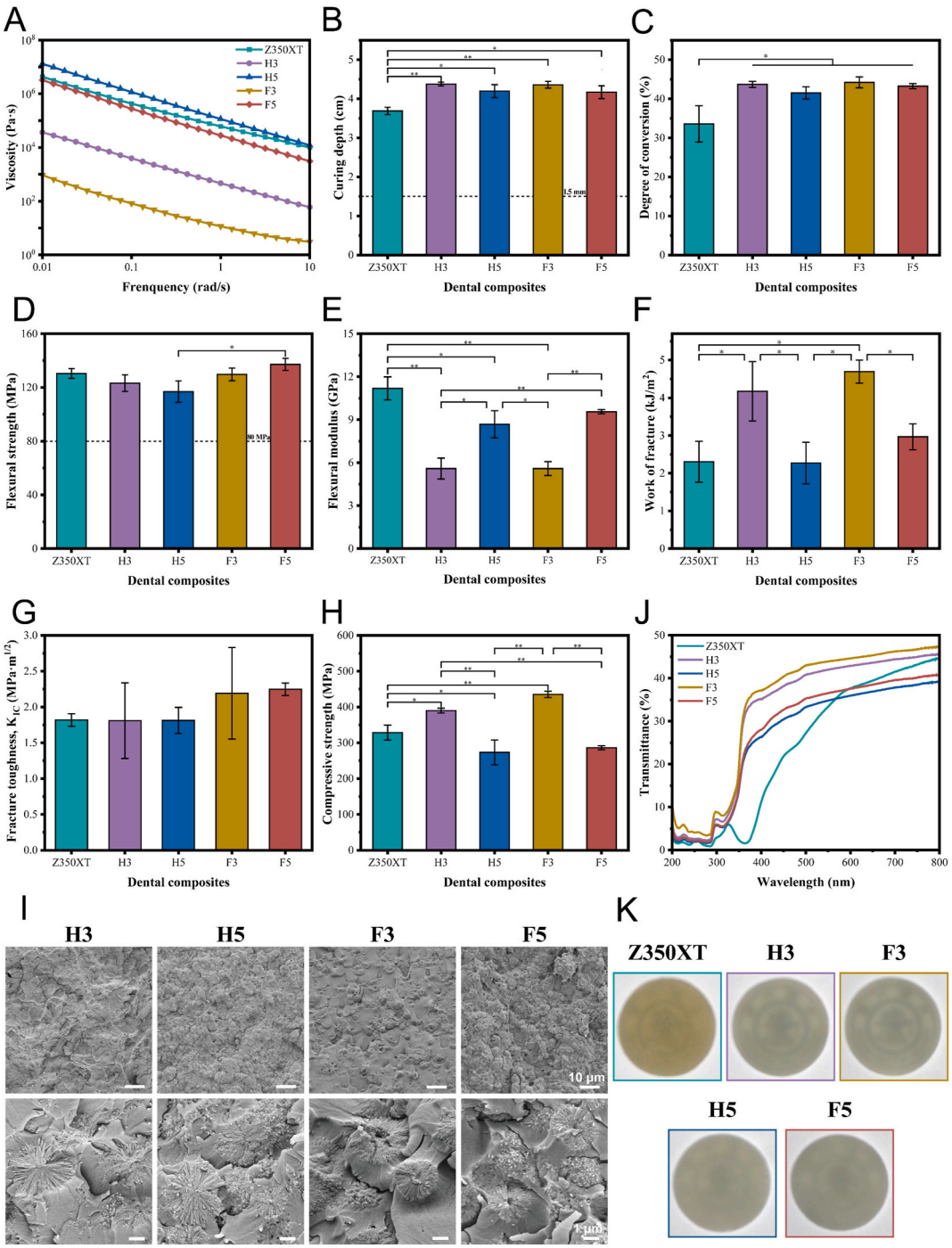


**Fig. 2.** Physicochemical properties of DRCs. Viscosity (A), curing depth (B), DC (C), FS (D), FM (E), WOF (F), $K_{IC}$ (G), CS (H), FE-SEM images of the fracture morphologies (excluding Z350XT), (I) spectral transmittance curves (J) and digital photos of the 1 mm thick disks (K) of Z350XT, H3, H5, F3 and F5. *$p < 0.05$, **$p < 0.001$.

behavior, and the viscosity of the 50 wt% filler loading DRCs was similar to that of Z350XT, favorable for extrusion from the syringe and the filling process. In addition, there was a discernible increase in the viscosity of the DRCs corresponding to the rise in filler loading, consistent with previous studies [53]. For DRCs with equivalent filler loading, the viscosity of FUHA groups was slightly lower than that of UHA groups. This difference was likely attributable to the slightly larger particle size and the denser whisker composition inherent to FUHA [54].

A higher curing depth of DRCs is also crucial for their clinical application, offering convenience for practitioners and reducing treatment time [55]. As shown in Fig. 2B, the curing depth value of each experimental DRC was higher than that of Z350XT, and far exceeded the requirement of ISO 4049-2019 (1.5mm). The DC of DRCs was measured to evaluate the extent of monomer polymerization, showing consistent with the curing depth finding (Fig. 2C). These results may be attributed to the low filler loading and large particle size of UHA or FUHA in DRCs [54,56]. The higher DC of UHA or FUHA-filled DRCs meant less unreacted monomer, which was beneficial to the improvement of mechanical strength and cytocompatibility [57,58]. In addition, the difference in refractive index between the filler and the resin matrix, led to the scattering of light, further reducing the DC of corresponding DRCs [59]. Therefore, the DC of 50 wt% filler loading DRCs was lower than

that of 30 wt%, although the difference was not significant.

The mechanical properties of DRCs are important indices for their use in dental restoration. Among all the DRCs, F5 presented the highest FS (137.17 ± 4.53 MPa) (Fig. 2D), which can be explained by the denser whisker structure of FUHA [45]. While, the FM was more closely related to filler content (Fig. 2E), with Z350XT showing the highest value due to its high filler loading of 78.5 wt% [60]. It is worth mentioning that at the same filling loading, the FM value of F5 (9.56 GPa) was higher than that of H5, showing no statistical difference from Z350XT.

DRCs' fracture is a major contributor to restoration failure, therefore, optimizing fracture behavior is crucial for improving the longevity of restorations [61]. The WOF of DRCs was measured and the results were shown in Fig. 2F. DRCs filled with 30 wt% loading presented better WOF compared to those with 50 wt% loading. This was mainly because the more long-chain soft organic resin matrix in H3 and F3 allowed for longer displacement before fracture (Fig. S2), thereby absorbing more energy [62]. By contrast, at the same filler content, the WOF of F5 increased by 30.40% compared to H5, suggesting that the more complex 3D whisker structure of FUHA particles dissipated more energy in the fracture process. Fracture toughness reflects the resistance of a material to crack extension under external loading [63]. Among all the DRCs, the fracture toughness of F3 and F5 presented 1.2 times higher than that of the other groups, although the difference was not statistically significant (Fig. 2G). This result suggested that the morphological structure of fillers in DRCs was an important factor affecting fracture toughness, where the denser whiskers of FUHA increase the crack surface area [64], resulting in improved fracture toughness. However, as shown in Fig. 2H, the CS values of F5 (286.11 MPa) and H5 (273.33 MPa) were relatively lower

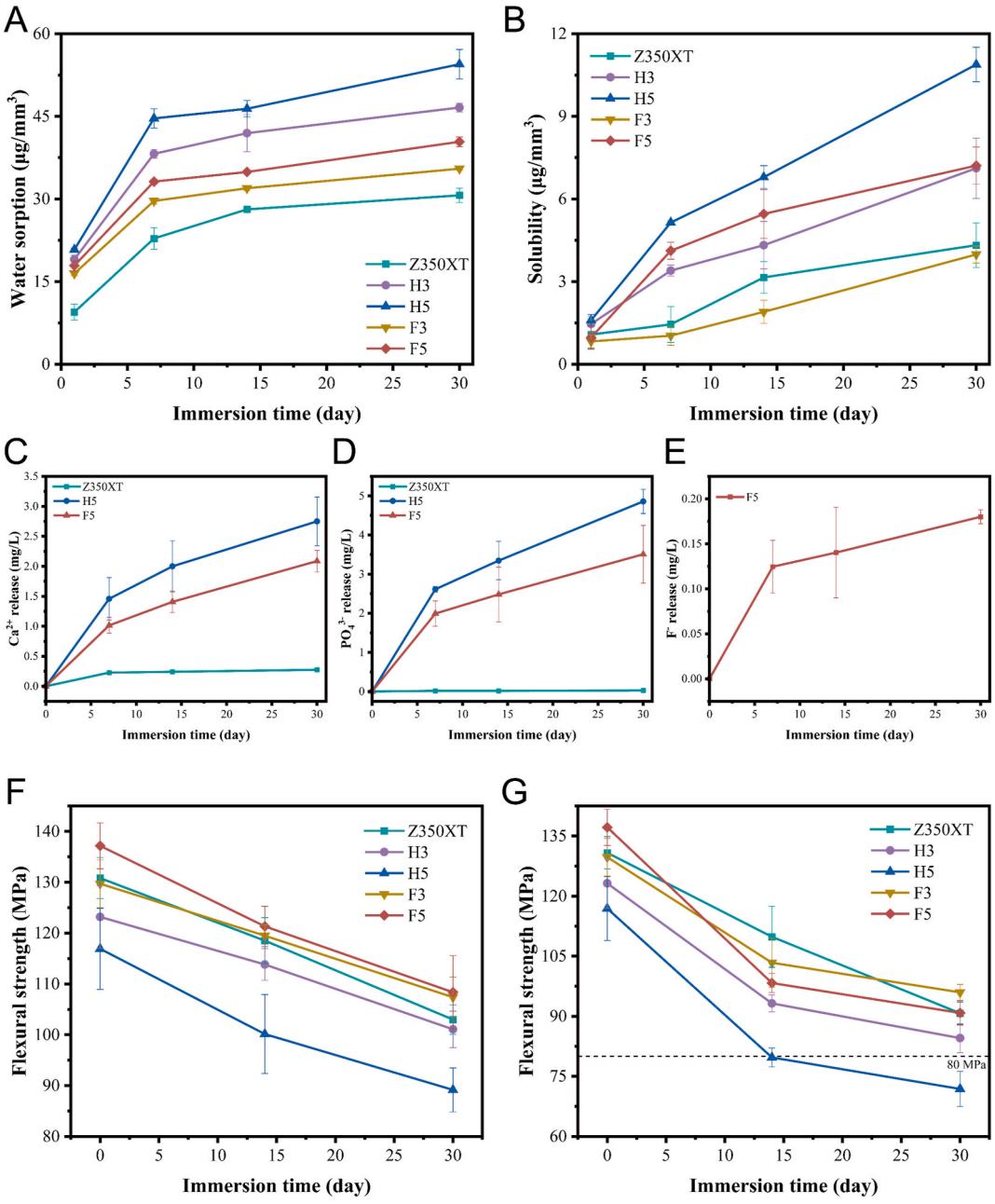


**Fig. 3.** Performance of DRCs in body-temperature and moist environments. (A) Water sorption and (B) solubility of Z350XT, H3, H5, F3 and F5 for 1, 7, 14, and 30 days. (C) Release of calcium ions and (D) phosphate from Z350XT, H5 and F5 for 7, 14, and 30 days. (E) Release of fluoride ions from F5 for 7, 14, and 30 days. (F) FS of Z350XT, H3, H5, F3 and F5 after soaking in SBF of pH = 7.4 for 0, 14, and 30 days. (G) FS of Z350XT, H3, H5, F3 and F5 after soaking in SBF of pH = 4 for 0, 14, and 30 days.

than those of F3 and H3. This difference may be attributed to the fact that high filler content lent to weaker interfacial interactions and particle agglomeration (Fig. 2I). In addition, the UHA or FUHA particles are brittle, which may also result the lower CS of corresponding DRCs. Nevertheless, it should be noted that the CS values of F5 and H5 were closer to the compressive strength of dentin (297.17 MPa) [65].

Based on all the above results of DRCs, F5 presented the best comprehensive mechanical properties. Similar to the relationship between plant roots and soil, the whisker structure of FUHA was conducive to embedding into the resin matrix and forming micromechanical interlocking at the fillers/resin matrix interface. When the DRCs were subjected to external force, the 1D whisker and the 3D urchin structure of FUHA would prevent crack propagation, requiring more external force to destroy the restorative materials. This could be demonstrated by the cross-sectional morphology of DRCs, as shown in Fig. 2I. The urchin-like fillers could form a three-dimensional embedded relationship with the resin matrix. Under force, three-dimensional whiskers could play whisker-enhancing roles such as crack deflection, whisker breakage, bridging and pullout in an all-around way [23]. Additionally, as can be seen from the SEM images (Fig. S3) of the dissolved fillers in H3, H5, F3 and F5, the separated UHA and FUHA particles from DRCs pastes still effectively maintained their complete urchin-like morphological structure, demonstrating that the SpeedMixer and three-roll mixer did not alter the morphological structure of the filler particles, which was beneficial for the reinforcement of DRCs.

The light transmission and aesthetic property of DRCs should also be considered [66]. As shown in Fig. 2J, the percentage of light transmitted of the DRCs as a function of incident wavelength revealed that the mass fraction of the urchin-like fillers affected the light transmission of the composites. The light transmission decreased with an increase in the filler loading from 30 wt% to 50 wt%, and the value of FUHA-filled DRCs was higher than that of UHA. This was further substantiated by digital photographs presented in Fig. 2K. Overall, the aesthetic of all four experimental DRCs was acceptable compared to Z350XT (Shade: A2B), laying a foundation for their potential dyeing and clinical applications.

### 3.3. Performance of DRCs in body-temperature and moist environments

The oral environment is moist, which requires DRCs to have excellent stability in wet, body-temperature environments. Therefore, the water absorption and solubility of DRCs were measured and the results were shown in Fig. 3A and B. Except for H5, the water absorption values of H3, F3, F5, and commercial Z350XT met the requirement of ISO 4049-2019, which were below 40 μg/mm$^3$ after 7 days in water [32]. And F5 exhibited a significant reduction in water absorption compared to H5, decreasing by 25.73%, 24.74%, and 25.83% at 7, 14, and 30 days of immersion, respectively. This suggested that fluorine incorporation could significantly improve DRCs' water absorption, which can be attributed to the low surface energy and small atomic radius of fluorine. The solubility of FUHA-filled DRCs also decreased compared with that of UHA-filled DRCs, where the values of F5 reducing by 39.23%, 42.23%, 19.69%, and 33.75% at 1, 7, 14, and 30 days, respectively, compared to H5. This optimization in solubility was attributed to the enhanced stability of FHA versus HA, and the tighter filler/resin matrix interface bonding [20].

Based on the acceptable solubility of H5 and F5, they were selected as a representative to further test the release of calcium, phosphorus, and fluoride ions in water or SBF, as these elements can facilitate the remineralization of dentin [67–69], and fluoride ions have antibacterial effects [28,70]. The results demonstrated that after soaking the DRCs in water for different time points, both H5 and F5 presented a pronounced release of calcium and phosphorus ions within the initial 7-day period, followed by a gradual and steady release (Fig. 3C and D), and the similar trend of fluoride ion release was detected in F5 (Fig. 3E). In comparison with F5, H5 exhibited a marginally higher ion release while this difference was not statistically significant ($P > 0.05$). This result was mainly attributed to the fluorine in F5, making FUHA more resistant to hydrolysis. And according to previous study, this initial release characteristic is beneficial to "replenishment and re-release of F" [71]. In addition, we further evaluated the ions release in the SBF, and the results showed that the ion releases of H5 and F5 were slightly lower than in the deionized water, while Z350XT had almost no ion release (Fig. S4). The release of functional ions from H5 and F5 was conducive to the realization of anti-caries function.

Furthermore, we also determined the mechanical stability property of DRCs after immersion in SBF at 37 °C. It was observed that the simulated oral environment predominantly affected the FS of DRCs (Fig. 3F) rather than their FM (Fig. S5), which was consistent with the previous studies [72]. After 30 days of immersion, the FS of Z350XT, H3, H5, F3, and F5 decreased by 21.28%, 17.96%, 23.74%, 17.21%, and 21.00%, respectively. It could be inferred that the mechanical stability of DRCs was closely related to the composition and structure of fillers. The DRCs that contain fillers with more soluble and weaker filler/resin matrix interface binding (e.g., 50% UHA) would result in greater reduction in mechanical strength. In an acidic oral simulant environment, mimicking cariogenic conditions, DRCs displayed a more pronounced early-stage decrease in strength and some decline in modulus (Fig. 3G and Fig. S5B), likely due to the increased solubility of fillers under acidic conditions and accelerated aging of the resin matrix [73]. In particular, the FS of H5 fell below 80 MPa within 14 days, which was mainly attributed to the high solubility of UHA. Conversely, F5 demonstrated superior mechanical stability even in acidic conditions, making it a favorable choice for restorative material in caries treatment, particularly in scenarios involving excessive intake of acidic foods.

### 3.4. Remineralization of DRCs

In response to caries-induced demineralization, the remineralization potential of DRCs, particularly H5 and F5, which exhibit superior physicochemical properties, was evaluated. Fig. 4A illustrated the surface morphology of various DRCs after soaking in SBF for different durations. Notably, Z350XT had almost no mineralization layer formation, even with prolonged soaking. In contrast, H5 and F5 demonstrated early signs of mineralization, forming aggregated spherical structures after only 1 day of immersion. After 14 days, F5's surface was entirely covered with a mineralized layer, whereas H5 exhibited partial coverage. Extending the immersion period to 30 days, both F5 and H5 presented thicker and denser mineralized layers. These results were consistent with previous finding that the incorporation of calcium and phosphorus into DRCs could enhance surface mineralization [74]. Additionally, the introduction of fluorine element expedited this process, potentially due to the facilitated nucleation and deposition of FHA [75]. Moreover, the presence of fluorine in DRCs also promoted the formation of a more substantial and complete mineralization layer in acidic conditions for 30 days (Fig. S6), endowing F5 with a superior capacity for mineral deposition in cariogenic environments.

DRCs are commonly applied to open dentin tubules resulting from tooth destruction or clinical acid erosion. Therefore, the remineralizing ability of different DRCs on demineralized dentin was further investigated. Fig. 4B revealed that treatment with both H5 and F5 resulted in closure of dentin tubules through new mineralization, whereas tubules remained open after Z350XT treatment. This result was further proved by the longitudinal profile of the dentin slices (Fig. S7), which revealed that F5 facilitated remineralization of the dentin tubules to a depth of approximately 20 μm and its remineralization quality surpassed that achieved with H5. However, no mineral formation was observed in Z350XT treated group. EDS analysis, as shown in Fig. 4C, indicated that H5 facilitated the deposition of calcium-phosphorus compounds within the tubules, which was consistent with the composition of intact dentin. Additionally, F5 treatment not only led to calcium and phosphorus deposition but also introduced fluorine, which could enhance the remineralized layer's resistance to acidic conditions. Furthermore, the

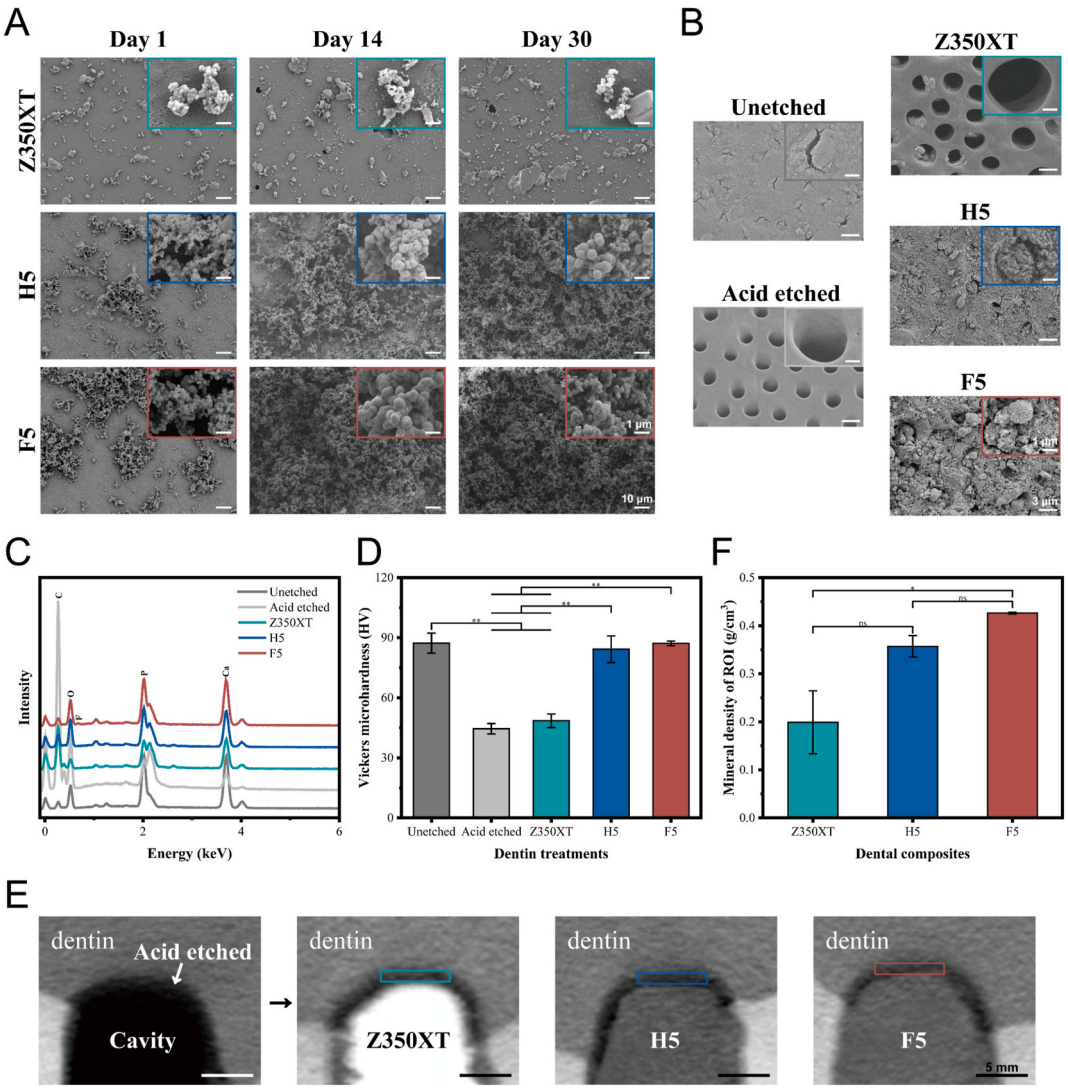


**Fig. 4.** Remineralization of DRCs. (A) FE-SEM images of surface morphologies of Z350XT, H5 and F5 after soaking in SBF for 1, 14, and 30 days. (B) FE-SEM images of dentin slices, demineralized dentin slices, and demineralized dentin slices being treated with Z350XT, H5, and F5 and soaked in SBF for 14 days. (C) EDS spectra of dentin tubules, demineralized dentin tubules, and demineralized dentin tubules treated with Z350XT, H5 and F5 and soaked in SBF for 14 days. (D) Vickers microhardness of dentin slices, demineralized dentin slices, and demineralized dentin slices being treated with Z350XT, H5, and F5 and soaked in SBF for 14 days. (E) Micro-CT images of artificial cavities and artificial cavities filled with Z350XT, H5 and F5 and soaked in SBF for 30 days. (F) Mineral densities in the original demineralized areas of the artificial cavities after being filled with Z350XT, H5, and F5 (boxed in Fig. 5E). *$p < 0.05$, **$p < 0.001$.

hardness of dentin slices treated with DRCs was assessed (Fig. 4D). Results showed that dentin hardness of F5 and H5 groups returned to a level comparable to undemineralized dentin, unlike the Z350XT group. The recovery in hardness was associated with the tubular remineralization [76].

In addition, Micro-CT scanning was utilized to visualize demineralized lesions in caries cavities and subsequent filling treatments [77–79]. In artificial dentin caries with a depth of around 200 μm, post-filling treatment analysis revealed high-density area in the previously demineralized zone (Fig. 4E), indicative of remineralization. Density measurements (Fig. 4F) revealed that F5 exhibited the highest remineralization capability, which was obviously better than Z350XT. Although H5 also contributed to the remineralization of demineralized dentin, its effectiveness was less pronounced than that of F5. These observations supported the conclusion that the ions released by F5 and H5 likely transformed into calcium-phosphorus-fluorine compounds, facilitating mineralization. This remineralization process served multiple purposes: filling micro-gaps between the tooth and the restoration, restoring the hardness of the tooth, as well as safeguarding the pulp [80,81].

### 3.5. Cell activity of DRCs

Through dentin tubules, the channels containing body fluids, DRCs have an impact on the health of the pulp, and the survival of pulp cells is critical to the success of dental restorations [82,83]. The impacts of DRCs with varying UHA or FUHA fillings on hDPSCs were assessed in accordance with ISO-10993. Fig. 5A presented the live/dead staining fluorescence images of hDPSCs exposed to different DRCs extracts. Promisingly, none of the samples exhibited notable cytotoxicity compared to the blank medium. Notably, H5 and F5 demonstrated a higher proportion of live cell staining, suggesting excellent biocompatibility. Quantitative analysis of the live (green) and dead (red) cell staining revealed that the survival rate of hDPSCs in all groups exceeded 98% at each time point (Fig. 5B). Particularly on day 7, the live cell counts in H5 and F5 groups surpassed those of the blank medium and the Z350XT group. The effects of various DRCs on the proliferation of hDPSCs were shown in Fig. 5C, as determined through CCK-8 assays.

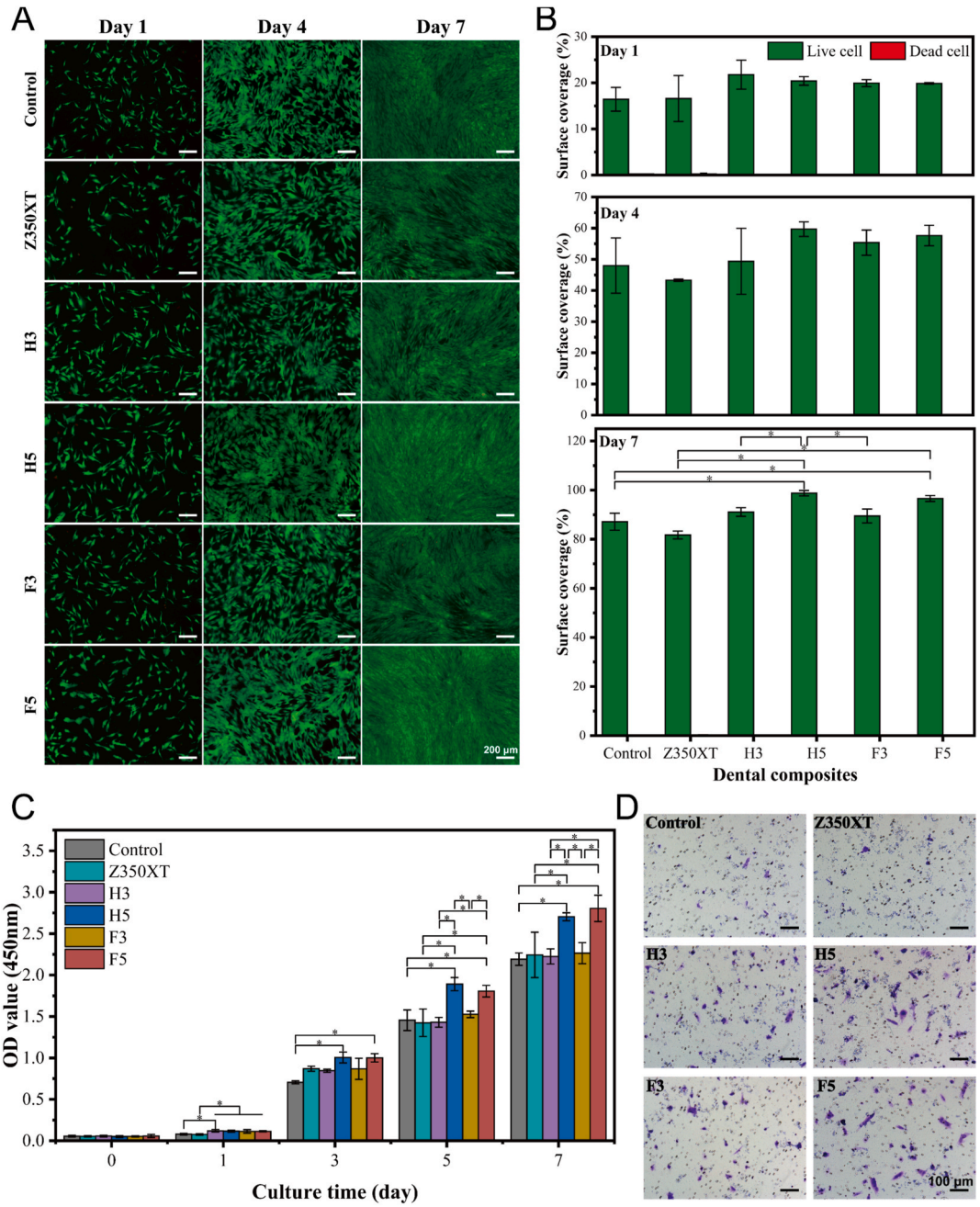


**Fig. 5.** Cell activity of DRCs. (A) Fluorescence microscopy images of live/dead staining of hDPSCs cultured in blank medium and Z350XT, H3, H5, F3, and F5 extracts for 1, 4, and 7 days: green (live) and red (dead). (B) Surface coverage of live and dead hDPSCs from evaluating fluorescent images with ImageJ software. (C) CCK-8 assay of hDPSCs cultured in blank medium and Z350XT, H3, H5, F3, and F5 extracts for 0, 1, 3, 5, and 7 days. (D) Migration assay of hDPSCs cultured in blank medium and Z350XT, H3, H5, F3, and F5 extracts for 24 h *$p < 0.05$.

Notably, DRCs composed of 50% UHA or FUHA were found to enhance cell proliferation, which was consistent with the results of live/dead staining. These increases in cell activity were due to the fact that HA and FHA were biologically active components. Extracts from these materials contain calcium and fluorine ions, which have been reported to favor the proliferation of hDPSCs [84,85].

Cell migration is the rate-limiting event for reestablishing pulp tissue and restoring normal function after pulp damage [86]. Given the risk of pulp exposure and damage associated with deep caries, the influence of DRCs containing bioactive components on hDPSCs migration was investigated using a transwell-migration assay. Fig. 5D demonstrated that hDPSCs exhibited varying degrees of migration in response to different extracts in the lower chamber. Notably, H3, H5, F3, and F5 significantly enhanced cell migration compared to both the blank and Z350XT control groups, with H5 and F5 showing a more pronounced effect (Fig. S8). This indicated that DRCs containing UHA and FUHA might promote hDPSCs migration towards the filling site (i.e., the carious lesion), potentially facilitating the pulpal defense response at the affected site [87,88].

### 3.6. *In vitro mineralized differentiation of hDPSCs*

As caries progress to the dentin, the pulp tissue can be activated to form a defense response due to the association of dentin tubules and pulp cells. Beyond the increased proliferation and migration of cells detailed earlier, the hDPSCs can differentiate to form mineralized tissues

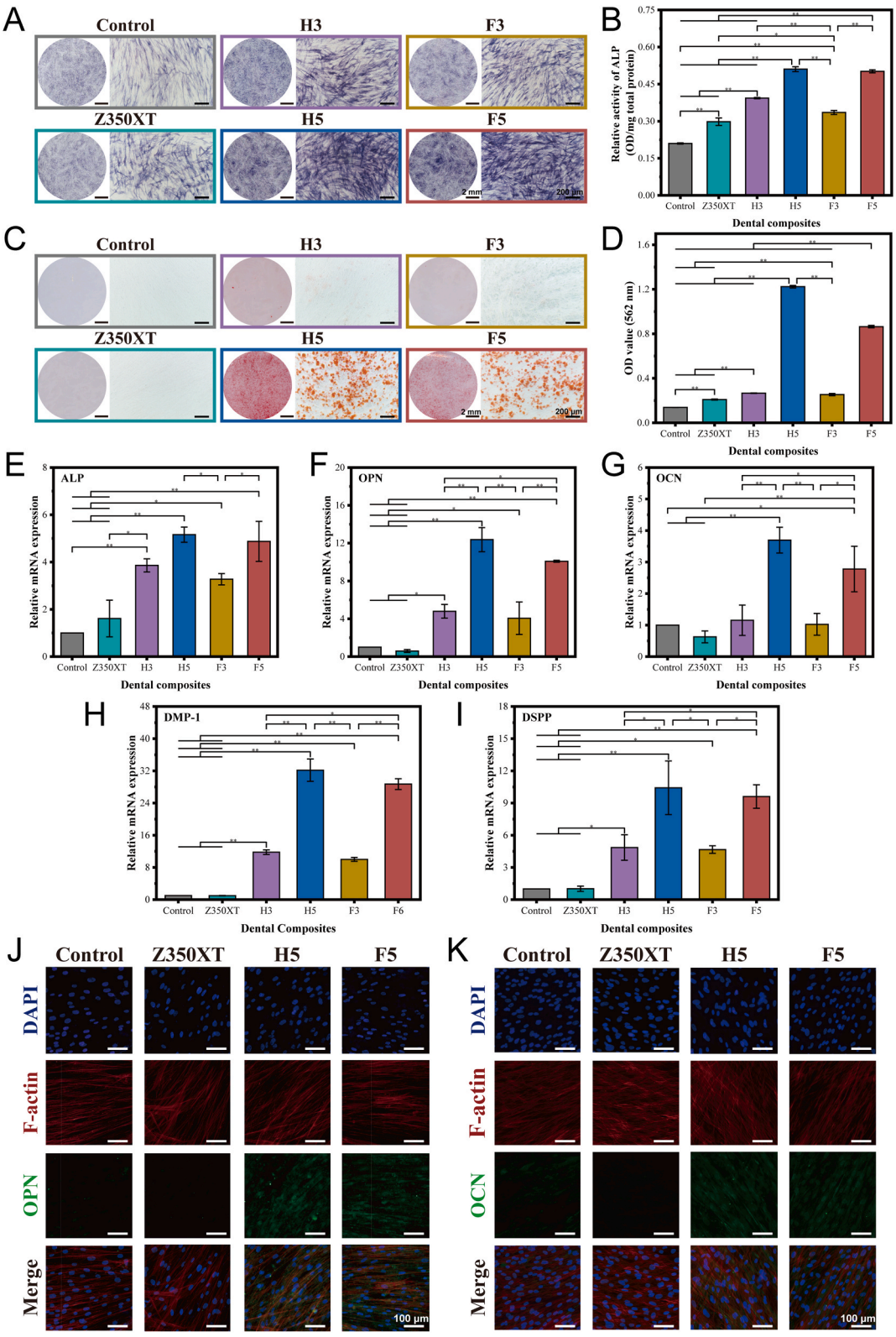


**Fig. 6.** Mineralized differentiation of hDPSCs *in vitro*. (A) ALP staining of hDPSCs and (B) semiquantitative analysis of ALP activity in hDPSCs cultured in osteogenic induction medium and Z350XT, H3, H5, F3, and F5 extracts for 14 days. (C) ARS staining of hDPSCs and (D) quantitative analysis of ARS staining of hDPSCs cultured in osteogenic induction medium and Z350XT, H3, H5, F3, and F5 extracts for 21 days. (E–I) The mRNA expression of ALP, OPN and OCN in hDPSCs cultured in osteogenic induction medium and Z350XT, H3, H5, F3, and F5 extracts for 14 days, while the mRNA expression of DMP-1 and DSPP in hDPSCs cultured for 21 days. (J, K) The immunofluorescence staining images of OPN and OCN in hDPSCs cultured in osteogenic induction medium and Z350XT, H5, and F5 extracts for 14 days: blue (DAPI), red (F-actin), green (OPN or OCN). *$p < 0.05$, **$p < 0.001$.

helping to alleviate pulpal sensitivity [89]. To verify the effect of DRCs filled with various contents of UHA and FUHA on hDPSC differentiation, cell cultures were performed with distinct inducible extracts. After 14 days, ALP staining resulted varied significantly across the groups (Fig. 6A). Notably, hDPSCs cultured with H5 and F5 extracts displayed deeper staining than other groups. Quantitative analysis of ALP protein, following cell lysis (Fig. 6B), revealed significantly higher ALP expression in the H5 and F5 groups compared to others, with discernible differences among the remaining groups. As ALP is an early indicator of mineralized differentiation [90], staining and quantitative analysis of ALP showed that DRCs containing more UHA and FUHA could achieve mineralization induction of hDPSCs by body fluid. Subsequently, extracellular mineral deposition was evaluated using ARS staining, and the results showed that calcium nodule formation was most pronounced in the H5 group, followed by F5, while other groups exhibited minimal nodules (Fig. 6C). The quantitative results (Fig. 6D) were in line with these observations. Considering the pivotal role of calcium and phosphorus ions in hard tissue mineralization, this differential mineral deposition could be closely linked to the ion content in the extracts [91]. The H5 extract, releasing more calcium and phosphorus ions, was more conducive to extracellular calcium nodule formation, followed by F5 [92–94]. In contrast, the H3 and F3 groups demonstrated weaker induction of cellular mineral deposition, likely due to lower bioactive component content and solubility.

Furthermore, genes associated with mineralization and odontogenic differentiation were detected by RT-PCR, specifically the ALP, OCN,

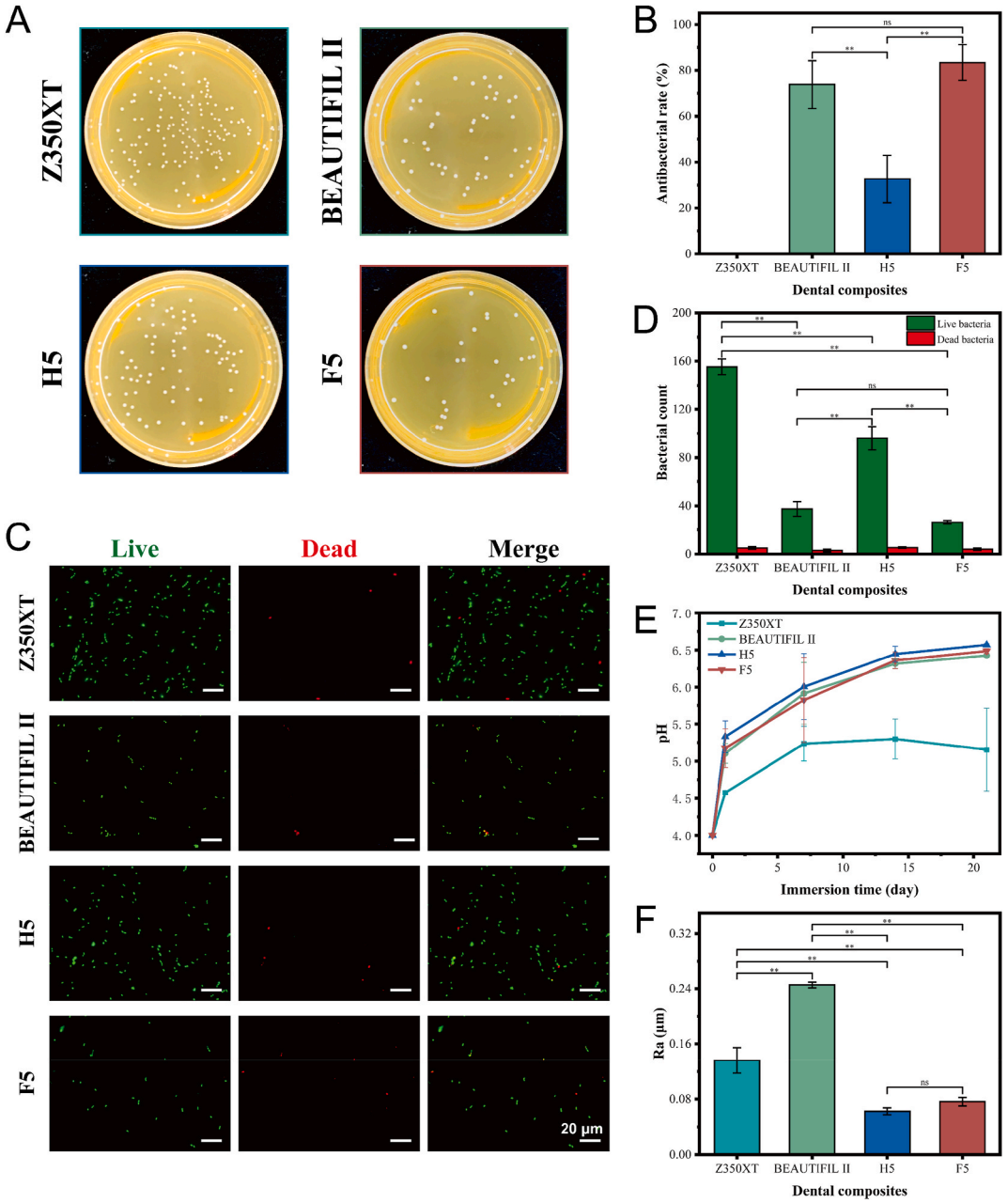


**Fig. 7.** Antibacterial effects and environment of DRCs. (A) Colonies of *S. mutans* eluted from the surfaces of Z350XT, BEAUTIFIL II, H5, and F5 after incubation. (B) Inhibition of *S. mutans* adhesion by BEAUTIFIL II, H5 and F5 with zero antibacterial rate of Z350XT. (C) Fluorescence microscopy images of live/dead staining of *S. mutans* cultured in Z350XT, BEAUTIFIL II, H5, and F5's cultures for 3 days. (D) Counts of live and dead bacteria using ImageJ software. (E) The solution pH of Z350XT, BEAUTIFIL II, H5, and F5 soaked in SBF at pH = 4 for 1, 7, 14, and 21 days. (F) Roughness of the surface of Z350XT, BEAUTIFIL II, H5, and F5 after 20 s of polishing. **p < 0.001.

OPN, DMP-1, and DSPP genes. Among them, ALP, OCN, and OPN are typical biomarkers of osteogenesis and odontogenesis, and DMP-1 and DSPP play crucial roles in dentin biomineralization [40,95]. For the ALP gene (Fig. 6E), up-regulation of its mRNA was achieved at 14 days using DRCs extracts of the experimental groups, especially H5 and F5, aligning with the results of ALP staining. Additionally, the experimental groups of DRCs also induced an up-regulation of the OPN gene at 14 days, also especially in the 50 wt% groups (Fig. 6G). OCN, a marker gene for late-stage mineralization [96], also showed significant up-regulation in the 50 wt% UHA-filled and 50 wt% FUHA-filled groups after 14 days of inducible culture (Fig. 6F). Genes critical to dentin formation manifested up-regulation later, with significant increases observed in the H5 and F5 groups at 21 days, consistent with previous studies [97,98]. In addition, the F5 group showed lower mineralized differentiation of cells than H5, which was mainly due to the lower release of calcium and phosphorus ions in F5. Finally, immunofluorescence staining more directly demonstrated (Fig. 6G and K) that the extracts of H5 and F5 significantly increased the expression of mineralization-associated proteins OCN and OPN, with more extensive and deeper staining. These findings suggested that DRCs containing UHA and FUHA, novel bioactive particles, were able to promote the mineralization of hDPSCs, thus contributing significantly to the protection of deep pulpal tissues and the restoration of dental hard tissues.

### 3.7. Antibacterial analysis of DRCs

Bacterial infection, mainly caused by *S. mutans*, is a primary cause of caries [99]. Although H5 and F5 treatments could hinder bacterial invasion pathways through remineralization, cariogenic bacteria may circumvent these barriers via acid production or microleakage in DRCs, leading to secondary caries. Consequently, the antibacterial activity of H5 and F5 was assessed, using commercial Z350XT as a negative control and BEAUTIFIL II as a positive control [100]. The bacterial spread plate test showed the number of bacteria adhering to the surfaces of different DRCs (Fig. 7A). Statistical analysis of the results (Fig. 7B) indicated that the DRCs containing FUHA had comparable or even higher antibacterial activity than BEAUTIFIL II, which was related to the widely reported ability of F element to inhibit the metabolism of bacteria [101]. Additionally, the bacterial survival in various DRCs-impregnated liquid environments was evaluated using bacterial live/dead staining. Fig. 7C and D revealed that the environments of BEAUTIFIL II, H5, and F5 significantly reduced the number of live *S. mutans*, while the count of dead bacteria changed little compared to the negative control. This suggested that these DRCs primarily inhibit growth and metabolism while being less capable of sterilizing. This was similar to previous studies in which calcium fluoride nanoparticles could inhibit *S. mutans*' enzyme activity as well as adhesion and other activities without damaging the bacterial cell membrane [102]. Further, the acid-neutralizing ability of different DRCs was evaluated. When immersed in an acid solution at pH = 4, H5, F5, and BUEATIFIL II sequentially increased the solution's pH (Fig. 7E). The acid neutralization effect of H5 and F5 might be due to the detachment of the hydroxyl group from the fillers and its interaction with hydrogen ions. The increasing pH could inhibit the proliferation of cariogenic bacteria, thereby offering protection to the teeth [103]. In addition, by comparing the polishability of different DRCs, H5 and F5 achieved significantly smoother surfaces than Z350XT and BEAUTIFIL II (Fig. 7F). This smoothness was attributed to the interfacial integrity provided by the 3D whisker structure of UHA and FUHA, preventing

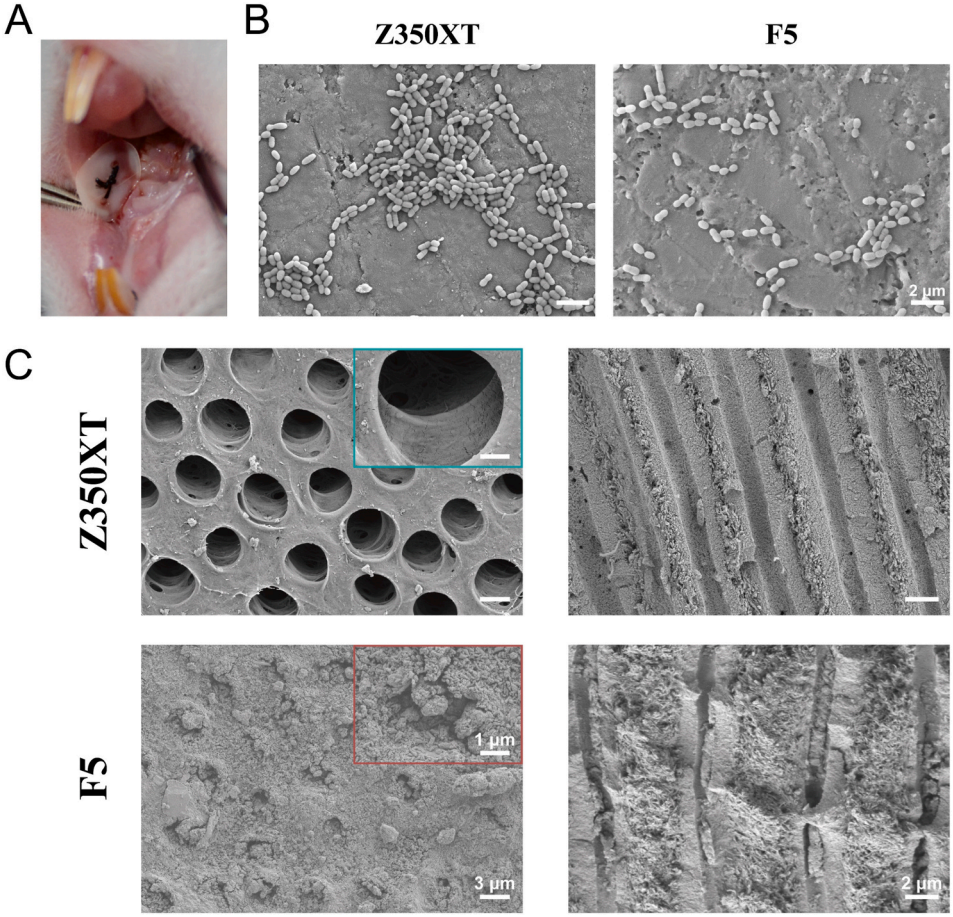


**Fig. 8.** *In vivo* effects of Z350XT and F5. (A) Demineralized dentin slices were fixed in the rat oral cavity. (B) FE-SEM image of *S. mutans* on the surface of Z350XT and F5. (C) FE-SEM image of the dentin slices and their longitudinal sections after Z350XT and F5 treatment.

large depressions during polishing. The smoother surfaces of the H5 and F5 were less conducive to bacterial adhesion, resulting in fewer bacteria on their surfaces [104].

### 3.8. In vivo effect evaluation

To evaluate the mineralization effect of F5 in simulated cariogenic oral environments, *in vivo* experiment was performed using commercial Z350XT as a control DRC. The demineralized dentin slices were fixed in the rat oral cavity (Fig. 8A), and then treated with Z350XT and F5, respectively. Meanwhile, a simulated cariogenic environment was created by giving the rats diet and coating *S. mutans* onto the materials. FE-SEM observation showed a large number of aggregated *S. mutans* on the surface of Z350XT, while the number of bacteria on the surface of F5 decreased significantly (Fig. 8B), indicating that F5 had better antibacterial property *in vivo*. Furthermore, the property of different DRCs on dentinal tubule remineralization was evaluated (Fig. 8C). In the control group, no occluded dentinal tubules were found, while the dentin slices treated with F5 displayed occluded tubules and the mineral deposits observed in the longitudinal sections of these tubules, as shown in the SEM images. These findings align with the above *in vitro* results, demonstrating that F5 can effectively remineralize dentin in cariogenic conditions *in vivo*. The combined antibacterial and remineralizing effects of F5 underscore its potential as a superior restorative material in combating dental caries.

## 4. Conclusion

Inspired by the plant root-soil interaction, DRCs constructed with the structure/function-integrated FUHA were developed in this study for the restorative treatment of cavitated dentin caries. FUHA exhibited an urchin-like 3D whisker structure and was composed of bioactive FHA. Similar to how roots stabilize soil, FUHA can be firmly embedded in the resin matrix and form micromechanical interlocking at the fillers/resin matrix interface, thereby endowing DRCs with superior physicochemical properties. In particular, F5 utilized FUHA to achieve exceptional curing properties, mechanical strength, and oral environment stability. Similar to the way roots nourish soil, FUHA-filled DRCs facilitated remineralization of dentin by releasing calcium, phosphorus, and fluoride ions, thereby preventing caries progression and promoting mineralized restoration. Furthermore, F5 exhibited bioactivity, enhancing the mineralized differentiation of hDPSCs and preventing bacterial adhesion and growth to protect dentin and the deep pulp. This novel FUHA-filled DRC effectively solved the issues of low fracture strength and non-bioactivity of current commercial DRCs, making it a promising restorative material for caries treatment, particularly for deep dentin caries.

## Ethics approval and consent to participate

All protocols were in accord with the guidelines set by the Ethics Committee of the Ninth People's Hospital Affiliated to Shanghai Jiaotong University School of Medicine (SH9H-2020-T298-3 and SH9H-2023-A794).

## CRediT authorship contribution statement

**Shuning Zhang:** Writing – original draft, Methodology, Investigation, Formal analysis, Conceptualization. **Xiao Wang:** Validation, Investigation, Methodology, Writing – original draft. **Shi Yin:** Writing – original draft, Validation, Methodology. **Junjun Wang:** Validation, Investigation. **Hongyan Chen:** Writing – review & editing, Supervision, Funding acquisition, Conceptualization. **Xinquan Jiang:** Writing – review & editing, Supervision, Investigation, Funding acquisition, Conceptualization.

## Declaration of competing interest

The authors declare no competing financial interests or personal relationships that could have appeared to influence the work reported in this paper.

## Acknowledgements

The authors acknowledge the support from the National Natural Science Foundation of China (Grant Nos. 82201115, 81921002), China Postdoctoral Science Foundation (No.2021M702166), and the Innovative Research Team of High-level Local Universities in Shanghai, Oral and Maxillofacial Regeneration and Functional Restoration.

## Appendix A. Supplementary data

Supplementary data to this article can be found online at https://doi.org/10.1016/j.bioactmat.2024.02.004.

## References

[1] N.B. Pitts, D.T. Zero, P.D. Marsh, K. Ekstrand, J.A. Weintraub, F. Ramos-Gomez, J. Tagami, S. Twetman, G. Tsakos, A. Ismail, Dental caries, Nat. Rev. Dis. Prim. 3 (2017) 17030, https://doi.org/10.1038/nrdp.2017.30.
[2] R.H. Selwitz, A.I. Ismail, N.B. Pitts, Dental caries, Lancet 369 (2007) 51–59, https://doi.org/10.1016/S0140-6736(07)60031-2.
[3] Y. Xu, Y. You, L. Yi, X. Wu, Y. Zhao, J. Yu, H. Liu, Y. Shen, J. Guo, C. Huang, Dental plaque-inspired versatile nanosystem for caries prevention and tooth restoration, Bioact. Mater. 20 (2023) 418–433, https://doi.org/10.1016/j.bioactmat.2022.06.010.
[4] R.M. Love, A.C.R. Tanner, in: A.F. Fouad (Ed.), Microbiology of Dental Caries and Dentinal Tubule Infection, first ed.Endod. Microbiol., John Wiley & Sons, Inc., Hoboken, 2017, pp. 25–49, https://doi.org/10.1002/9781119080343.ch3.
[5] L. Cheng, L. Zhang, L. Yue, J. Ling, M. Fan, D. Yang, Z. Huang, Y. Niu, J. Liu, J. Zhao, Y. Li, B. Guo, Z. Chen, X. Zhou, Expert consensus on dental caries management, Int. J. Oral Sci. 14 (2022) 17, https://doi.org/10.1038/s41368-022-00167-3.
[6] L. Tjäderhane, M.R. Carrilho, L. Breschi, F.R. Tay, D.H. Pashley, Dentin basic structure and composition-an overview, Endod. Top. 20 (2009) 3–29, https://doi.org/10.1111/j.1601-1546.2012.00269.x.
[7] G. Conrads, I. About, Pathophysiology of dental caries, in: F. Schwendicke, J. Frencken, N. Innes (Eds.), Caries Excav. Evol. Treat. Cavitated Carious Lesions, Karger, Basel, 2018, pp. 1–10, https://doi.org/10.1159/000487826.
[8] S. Zhang, X. Wang, J. Yang, H. Chen, X. Jiang, Micromechanical interlocking structure at the filler/resin interface for dental composites: a review, Int. J. Oral Sci. 15 (2023) 21, https://doi.org/10.1038/s41368-023-00226-3.
[9] J.L. Drummond, Degradation, fatigue, and failure of resin dental composite materials, J. Dent. Res. 87 (2008) 710–719, https://doi.org/10.1177/154405910808700802.
[10] A.A. Balhaddad, A.A. Kansara, D. Hidan, M.D. Weir, H.H.K. Xu, M.A.S. Melo, Toward dental caries: exploring nanoparticle-based platforms and calcium phosphate compounds for dental restorative materials, Bioact. Mater. 4 (2019) 43–55, https://doi.org/10.1016/j.bioactmat.2018.12.002.
[11] K. Cho, G. Rajan, P. Farrar, L. Prentice, B.G. Prusty, Dental resin composites: a review on materials to product realizations, Composites, Part B 230 (2022) 109495, https://doi.org/10.1016/j.compositesb.2021.109495.
[12] A. Aminoroaya, R.E. Neisiany, S.N. Khorasani, P. Panahi, O. Das, H. Madry, M. Cucchiarini, S. Ramakrishna, A review of dental composites: challenges, chemistry aspects, filler influences, and future insights, Composites, Part B 216 (2021) 108852, https://doi.org/10.1016/j.compositesb.2021.108852.
[13] J. Liu, H. Zhang, H. Sun, Y. Liu, W. Liu, B. Su, S. Li, The development of filler morphology in dental resin composites: a review, Materials 14 (2021) 5612, https://doi.org/10.3390/ma14195612.
[14] F. Elfakhri, R. Alkahtani, C. Li, J. Khaliq, Influence of filler characteristics on the performance of dental composites: a comprehensive review, Ceram. Int. 48 (2022) 27280–27294, https://doi.org/10.1016/j.ceramint.2022.06.314.
[15] Y. Wang, M. Zhu, X.X. Zhu, Functional fillers for dental resin composites, Acta Biomater. 122 (2021) 50–65, https://doi.org/10.1016/j.actbio.2020.12.001.
[16] Z. Liu, X. Wang, D. Qi, C. Xu, J. Yu, Y. Liu, Y. Jiang, B. Liedberg, X. Chen, High-adhesion stretchable electrodes based on nanopile interlocking, Adv. Mater. 29 (2017) 1603382, https://doi.org/10.1002/adma.201603382.
[17] M. Zhu, F. Zhang, X. Chen, Bioinspired mechanically interlocking structures, Small Struct 1 (2020) 2000045, https://doi.org/10.1002/sstr.202000045.
[18] C. Lv, C. Wang, A. Cai, Z. Zhou, Global magnitude of rhizosphere effects on soil microbial communities and carbon cycling in natural terrestrial ecosystems, Sci. Total Environ. 856 (2023) 158961, https://doi.org/10.1016/j.scitotenv.2022.158961.
[19] X. Zhao, P. Tian, Z. Sun, S. Liu, Q. Wang, Z. Zeng, Rhizosphere effects on soil organic carbon processes in terrestrial ecosystems: a meta-analysis, Geoderma 412 (2022) 115739, https://doi.org/10.1016/j.geoderma.2022.115739.

[20] K. Pajor, L. Pajchel, J. Kolmas, Hydroxyapatite and fluorapatite in conservative dentistry and oral implantology-A review, Materials 12 (2019) 2683, https://doi.org/10.3390/ma12172683.

[21] H.H.K. Xu, J.B. Quinn, D.T. Smith, A.A. Giuseppetti, F.C. Eichmiller, Effects of different whiskers on the reinforcement of dental resin composites, Dent. Mater. 19 (2003) 359–367, https://doi.org/10.1016/S0109-5641(02)00078-7.

[22] M. Cao, C. Zhang, J. Wei, Microscopic reinforcement for cement based composite materials, Construct. Build. Mater. 40 (2013) 14–25, https://doi.org/10.1016/j.conbuildmat.2012.10.012.

[23] F. Liu, B. Sun, X. Jiang, S.S. Aldeyab, Q. Zhang, M. Zhu, Mechanical properties of dental resin/composite containing urchin-like hydroxyapatite, Dent. Mater. 30 (2014) 1358–1368, https://doi.org/10.1016/j.dental.2014.10.003.

[24] F. Huo, Z. Jin, D. Le Han, K. Zhang, H. Nishikawa, Interface design and the strengthening-ductility behavior of tetra-needle-like ZnO whisker reinforced Sn1.0Ag0.5Cu composite solders prepared with ultrasonic agitation, Mater. Des. 210 (2021) 110038, https://doi.org/10.1016/j.matdes.2021.110038.

[25] W. Chang-an, H. Yong, Z. Hongxiang, The effect of whisker orientation in SiC whisker-reinforced $Si_3N_4$ ceramic matrix composites, J. Eur. Ceram. Soc. 19 (1999) 1903–1909, https://doi.org/10.1016/S0955-2219(98)00289-1.

[26] P. Makvandi, U. Josic, M. Delfi, F. Pinelli, V. Jahed, E. Kaya, M. Ashrafizadeh, A. Zarepour, F. Rossi, A. Zarrabi, T. Agarwal, E.N. Zare, M. Ghomi, T. Kumar Maiti, L. Breschi, F.R. Tay, Drug delivery (nano)platforms for oral and dental applications: tissue regeneration, infection control, and cancer management, Adv. Sci. 8 (2021) 2004014, https://doi.org/10.1002/advs.202004014.

[27] A. Bianco, I. Cacciotti, M. Lombardi, L. Montanaro, E. Bemporad, M. Sebastiani, F-substituted hydroxyapatite nanopowders: thermal stability, sintering behaviour and mechanical properties, Ceram. Int. 36 (2010) 313–322, https://doi.org/10.1016/j.ceramint.2009.09.007.

[28] J. Flemming, C. Hannig, M. Hannig, Caries managemen-The role of surface interactions in de- and remineralization-processes, J. Clin. Med. 11 (2022) 7044, https://doi.org/10.3390/jcm11237044.

[29] H. Qu, M. Wei, The effect of fluoride contents in fluoridated hydroxyapatite on osteoblast behavior, Acta Biomater. 2 (2006) 113–119, https://doi.org/10.1016/j.actbio.2005.09.003.

[30] H.-W. Kim, E.-J. Lee, H.-E. Kim, V. Salih, J.C. Knowles, Effect of fluoridation of hydroxyapatite in hydroxyapatite-polycaprolactone composites on osteoblast activity, Biomaterials 26 (2005) 4395–4404, https://doi.org/10.1016/j.biomaterials.2004.11.008.

[31] T. Guo, Y. Li, G. Cao, Z. Zhang, S. Chang, A. Czajka-Jakubowska, J.E. Nör, B. H. Clarkson, J. Liu, Fluorapatite-modified scaffold on dental pulp stem cell mineralization, J. Dent. Res. 93 (2014) 1290–1295, https://doi.org/10.1177/0022034514547914.

[32] ISO 4049-2019, Dentistry-Polymer-based Restorative Materials, 2019.

[33] L. Zhang, Z. Ma, R. Wang, W. Zuo, M. Zhu, Bis-quaternary ammonium betulin-based dimethacrylate: synthesis, characterization, and application in dental restorative resins, Mater. Adv. 4 (2023) 2127–2137, https://doi.org/10.1039/D3MA00016H.

[34] F. López-Suevos, S.H. Dickens, Degree of cure and fracture properties of experimental acid-resin modified composites under wet and dry conditions, Dent. Mater. 24 (2008) 778–785, https://doi.org/10.1016/j.dental.2007.09.006.

[35] J. Thadathil Varghese, K. Cho, Raju, P. Farrar, L. Prentice, B.G. Prusty, Effect of silane coupling agent and concentration on fracture toughness and water sorption behaviour of fibre-reinforced dental composites, Dent. Mater. 39 (2023) 362–371, https://doi.org/10.1016/j.dental.2023.03.002.

[36] H. Yli-Urpo, L.V.J. Lassila, T. Närhi, P.K. Vallittu, Compressive strength and surface characterization of glass ionomer cements modified by particles of bioactive glass, Dent. Mater. 21 (2005) 201–209, https://doi.org/10.1016/j.dental.2004.03.006.

[37] F.W. Liu, J.H. Hu, R.L. Wang, Y.Y. Pan, X.Z. Jiang, M.F. Zhu, Effect of filler ratio on properties of nanohydroxyapatite/$SiO_2$ based bioactive dental resin composites, Mater. Sci. Forum (2013) 466–472. https://doi.org/10.4028/www.scientific.net/MSF.745-746.466, 745–746.

[38] F.R. Tay, D.H. Pashley, Guided tissue remineralisation of partially demineralised human dentine, Biomaterials 29 (2008) 1127–1137, https://doi.org/10.1016/j.biomaterials.2007.11.001.

[39] F. Schwendicke, A. Al-Abdi, A. Pascual Moscardó, A. Ferrando Cascales, S. Sauro, Remineralization effects of conventional and experimental ion-releasing materials in chemically or bacterially-induced dentin caries lesions, Dent. Mater. 35 (2019) 772–779, https://doi.org/10.1016/j.dental.2019.02.021.

[40] N. Sun, S. Yin, Y. Lu, W. Zhang, X. Jiang, Graphene oxide-coated porous titanium for pulp sealing: an antibacterial and dentino-inductive restorative material, J. Mater. Chem. B 8 (2020) 5606–5619, https://doi.org/10.1039/D0TB00697A.

[41] ISO 10993-12, Biological Evaluation of Medical Devices-Part 12: Sample Preparation and Reference Materials, 2021, p. 2021.

[42] Z. Wu, H. Xu, W. Xie, M. Wang, C. Wang, C. Gao, F. Gu, J. Liu, J. Fu, Study on a novel antibacterial light-cured resin composite containing nano-MgO, Colloids Surf. B Biointerfaces 188 (2020) 110774, https://doi.org/10.1016/j.colsurfb.2020.110774.

[43] Y. Wang, C. Wu, K. Lin, J. Chang, Facile fabrication of nanorod-assembled fluorine-substituted hydroxyapatite (FHA) microspheres, Chem. Asian J. 8 (2013) 990–996, https://doi.org/10.1002/asia.201201233.

[44] M. Shen, G. Liang, A. Gu, L. Yuan, Development of high performance dental resin composites with outstanding antibacterial activity, high mechanical properties and low polymerization shrinkage based on a $SiO_2$ hybridized tetrapod-like zinc oxide whisker with C=C bonds, RSC Adv. 6 (2016) 56353–56364, https://doi.org/10.1039/C6RA13498J.

[45] H. Chen, J. Wang, R. Wang, M. Zhu, Synthesis of fluorinated urchin-like serried hydroxyapatite with improved water sorption-solubility and bioactivity for dental composites, Chem. Res. Chin. Univ. 37 (2021) 1092–1100, https://doi.org/10.1007/s40242-021-1268-2.

[46] J. Brzezińska-Miecznik, P. Jeleń, K. Haberko, W. Mozgawa, M. Sitarz, The effect of NaOH and KOH treatment on the behavior of $CO_3^{2-}$ and $OH^-$ groups in natural origin hydroxyapatite, Ceram. Int. 43 (2017) 12540–12545, https://doi.org/10.1016/j.ceramint.2017.06.127.

[47] C.-C. Wu, S.-T. Huang, T.-W. Tseng, Q.-L. Rao, H.-C. Lin, FT-IR and XRD investigations on sintered fluoridated hydroxyapatite composites, J. Mol. Struct. 979 (2010) 72–76, https://doi.org/10.1016/j.molstruc.2010.06.003.

[48] M.M. Nazarabady, G. Farzi, Morphology control to design p(acrylic acid)/silica nanohybrids with controlled mechanical properties, Polymer 143 (2018) 289–297, https://doi.org/10.1016/j.polymer.2018.02.026.

[49] B. Chen, Z. Lu, H. Meng, Y. Chen, L. Yang, H. Zhang, H. Xie, C. Chen, Effectiveness of pre-silanization in improving bond performance of universal adhesives or self-adhesive resin cements to silica-based ceramics: chemical and in vitro evidences, Dent. Mater. 35 (2019) 543–553, https://doi.org/10.1016/j.dental.2019.01.010.

[50] P. Saen, M. Atai, A. Nodehi, L. Solhi, Physical characterization of unfilled and nanofilled dental resins: static versus dynamic mechanical properties, Dent. Mater. 32 (2016) e185–e197, https://doi.org/10.1016/j.dental.2016.06.001.

[51] C.H. Zanchi, F.A. Ogliari, R. Marques E Silva, R.G. Lund, H.H. Machado, C. Prati, N.L.V. Carreño, E. Piva, Effect of the silane concentration on the selected properties of an experimental microfilled composite resin, Appl. Adhes. Sci. 3 (2015) 27, https://doi.org/10.1186/s40563-015-0054-0.

[52] J.-H. Lee, C.-M. Um, I. Lee, Rheological properties of resin composites according to variations in monomer and filler composition, Dent. Mater. 22 (2006) 515–526, https://doi.org/10.1016/j.dental.2005.05.008.

[53] D.F. Taylor, S. Kalachandra, M. Sankarapandian, J.E. McGrath, Relationship between filler and matrix resin characteristics and the properties of uncured composite pastes, Biomaterials 19 (1998) 197–204, https://doi.org/10.1016/S0142-9612(98)80001-X.

[54] E. Habib, R. Wang, X.X. Zhu, Correlation of resin viscosity and monomer conversion to filler particle size in dental composites, Dent. Mater. 34 (2018) 1501–1508, https://doi.org/10.1016/j.dental.2018.06.008.

[55] S. Flury, S. Hayoz, A. Peutzfeldt, J. Hüsler, A. Lussi, Depth of cure of resin composites: is the ISO 4049 method suitable for bulk fill materials? Dent. Mater. 28 (2012) 521–528, https://doi.org/10.1016/j.dental.2012.02.002.

[56] X. Li, P. Pongprueksa, B. Van Meerbeek, J. De Munck, Curing profile of bulk-fill resin-based composites, J. Dent. 43 (2015) 664–672, https://doi.org/10.1016/j.jdent.2015.01.002.

[57] J.L. Ferracane, E.H. Greener, The effect of resin formulation on the degree of conversion and mechanical properties of dental restorative resins, J. Biomed. Mater. Res. 20 (1986) 121–131, https://doi.org/10.1002/jbm.820200111.

[58] N.J. Walters, W. Xia, V. Salih, P.F. Ashley, A.M. Young, Poly(propylene glycol) and urethane dimethacrylates improve conversion of dental composites and reveal complexity of cytocompatibility testing, Dent. Mater. 32 (2016) 264–277, https://doi.org/10.1016/j.dental.2015.11.017.

[59] N. Emami, M. Sjödahl, K.-J.M. Söderholm, How filler properties, filler fraction, sample thickness and light source affect light attenuation in particulate filled resin composites, Dent. Mater. 21 (2005) 721–730, https://doi.org/10.1016/j.dental.2005.01.002.

[60] R. Wang, M. Zhang, F. Liu, S. Bao, T. Wu, X. Jiang, Q. Zhang, M. Zhu, Investigation on the physical-mechanical properties of dental resin composites reinforced with novel bimodal silica nanostructures, Mater. Sci. Eng. C 50 (2015) 266–273, https://doi.org/10.1016/j.msec.2015.01.090.

[61] J.L. Ferracane, Resin-based composite performance: are there some things we can't predict? Dent. Mater. 29 (2013) 51–58, https://doi.org/10.1016/j.dental.2012.06.013.

[62] X. Wu, Y. Sun, W. Xie, Y. Liu, X. Song, Development of novel dental nanocomposites reinforced with polyhedral oligomeric silsesquioxane (POSS), Dent. Mater. 26 (2010) 456–462, https://doi.org/10.1016/j.dental.2009.11.161.

[63] N. Ilie, R. Hickel, A.S. Valceanu, K.C. Huth, Fracture toughness of dental restorative materials, Clin. Oral Invest. 16 (2012) 489–498, https://doi.org/10.1007/s00784-011-0525-z.

[64] H.H.K. Xu, J.B. Quinn, D.T. Smith, J.M. Antonucci, G.E. Schumacher, F. C. Eichmiller, Dental resin composites containing silica-fused whiskers-effects of whisker-to-silica ratio on fracture toughness and indentation properties, Biomaterials 23 (2002) 735–742, https://doi.org/10.1016/S0142-9612(01)00178-8.

[65] R.G. Craig, F.A. Peyton, Elastic and mechanical properties of human dentin, J. Dent. Res. 37 (1958) 710–718, https://doi.org/10.1177/00220345580370041801.

[66] Z. Li, J. Wang, H. Chen, R. Wang, M. Zhu, Synthesis of ZnO nanorod-decorated graphene oxide for application in dental resin composites, ACS Biomater. Sci. Eng. 9 (2023) 2706–2715, https://doi.org/10.1021/acsbiomaterials.2c01523.

[67] M.D. Weir, J. Ruan, N. Zhang, L.C. Chow, K. Zhang, X. Chang, Y. Bai, H.H.K. Xu, Effect of calcium phosphate nanocomposite on in vitro remineralization of human dentin lesions, Dent. Mater. 33 (2017) 1033–1044, https://doi.org/10.1016/j.dental.2017.06.015.

[68] M. Iafisco, L. Degli Esposti, G.B. Ramírez-Rodríguez, F. Carella, J. Gómez-Morales, A.C. Ionescu, E. Brambilla, A. Tampieri, J.M. Delgado-López, Fluoride-doped amorphous calcium phosphate nanoparticles as a promising biomimetic material for dental remineralization, Sci. Rep. 8 (2018) 17016, https://doi.org/10.1038/s41598-018-35258-x.

[69] S.H. Dickens, G.M. Flaim, S. Takagi, Mechanical properties and biochemical activity of remineralizing resin-based Ca–$PO_4$ cements, Dent. Mater. 19 (2003) 558–566, https://doi.org/10.1016/S0109-5641(02)00105-7.
[70] L. Cheng, M.D. Weir, H.H.K. Xu, A.M. Kraigsley, N.J. Lin, S. Lin-Gibson, X. Zhou, Antibacterial and physical properties of calcium-phosphate and calcium-fluoride nanocomposites with chlorhexidine, Dent. Mater. 28 (2012) 573–583, https://doi.org/10.1016/j.dental.2012.01.006.
[71] A. Wiegand, W. Buchalla, T. Attin, Review on fluoride-releasing restorative materials-Fluoride release and uptake characteristics, antibacterial activity and influence on caries formation, Dent. Mater. 23 (2007) 343–362, https://doi.org/10.1016/j.dental.2006.01.022.
[72] H. Chen, J. Luo, J. Yang, C. Zeng, X. Jiang, Synthesis of pore-size-tunable porous silica particles and their effects on dental resin composites, Biomolecules 13 (2023) 1290, https://doi.org/10.3390/biom13091290.
[73] A. Szczesio-Wlodarczyk, J. Sokolowski, J. Kleczewska, K. Bociong, Ageing of dental composites based on methacrylate resins-A critical review of the causes and method of assessment, Polymers 12 (2020) 882, https://doi.org/10.3390/polym12040882.
[74] L. Qin, S. Yao, W. Meng, J. Zhang, R. Shi, C. Zhou, J. Wu, Novel antibacterial dental resin containing silanized hydroxyapatite nanofibers with remineralization capability, Dent. Mater. 38 (2022) 1989–2002, https://doi.org/10.1016/j.dental.2022.11.014.
[75] Z. Wang, G. Ma, X.Y. Liu, Will fluoride toughen or weaken our teeth? Understandings based on nucleation, morphology, and structural assembly, J. Phys. Chem. B 113 (2009) 16393–16399, https://doi.org/10.1021/jp905846p.
[76] K. Liang, S. Xiao, J. Wu, J. Li, M.D. Weir, L. Cheng, M.A. Reynolds, X. Zhou, H.H. K. Xu, Long-term dentin remineralization by poly(amido amine) and rechargeable calcium phosphate nanocomposite after fluid challenges, Dent. Mater. 34 (2018) 607–618, https://doi.org/10.1016/j.dental.2018.01.001.
[77] P.M. Pires, T.P. Santos, A. Fonseca-Gonc, A.A. Neves, Mineral density in carious dentine after treatment with calcium silicates and polyacrylic acid-based cements, Int. Endod. J. 51 (2018) 1292–1300, https://doi.org/10.1111/iej.12941.
[78] E.C.M. Lo, Q.H. Zhi, A. Itthagarun, Comparing two quantitative methods for studying remineralization of artificial caries, J. Dent. 38 (2010) 352–359, https://doi.org/10.1016/j.jdent.2010.01.001.
[79] A.J. Olejniczak, F.E. Grine, Assessment of the accuracy of dental enamel thickness measurements using microfocal X-ray computed tomography, Anat Rec A Discov Mol Cell Evol Biol 288A (2006) 263–275, https://doi.org/10.1002/ar.a.20307.
[80] K. Liang, Y. Gao, S. Xiao, F.R. Tay, M.D. Weir, X. Zhou, T.W. Oates, C. Zhou, J. Li, H.H.K. Xu, Poly(amido amine) and rechargeable adhesive containing calcium phosphate nanoparticles for long-term dentin remineralization, J. Dent. 85 (2019) 47–56, https://doi.org/10.1016/j.jdent.2019.04.011.
[81] J. Yu, H. Bian, Y. Zhao, J. Guo, C. Yao, H. Liu, Y. Shen, H. Yang, C. Huang, Epigallocatechin-3-gallate/mineralization precursors co-delivery hollow mesoporous nanosystem for synergistic manipulation of dentin exposure, Bioact. Mater. 23 (2023) 394–408, https://doi.org/10.1016/j.bioactmat.2022.11.018.
[82] L. Bjørndal, S. Simon, P.L. Tomson, H.F. Duncan, Management of deep caries and the exposed pulp, Int. Endod. J. 52 (2019) 949–973, https://doi.org/10.1111/iej.13128.
[83] I. About, P.E. Murray, J.-C. Franquin, M. Remusat, A.J. Smith, The effect of cavity restoration variables on odontoblast cell numbers and dental repair, J. Dent. 29 (2001) 109–117, https://doi.org/10.1016/S0300-5712(00)00067-1.
[84] I. Gurucharan, B. Saravana Karthikeyan, S. Mahalaxmi, K. Baskar, G. Rajkumar, V. Dhivya, A. Kishen, S. Sankaranarayanan, N. Gurucharan, Characterization of nano-hydroxyapatite incorporated carboxymethyl chitosan composite on human dental pulp stem cells, Int. Endod. J. 56 (2023) 486–501, https://doi.org/10.1111/iej.13885.
[85] L. Tammaro, V. Vittoria, A. Calarco, O. Petillo, F. Riccitiello, G. Peluso, Effect of layered double hydroxide intercalated with fluoride ions on the physical, biological and release properties of a dental composite resin, J. Dent. 42 (2014) 60–67, https://doi.org/10.1016/j.jdent.2013.10.019.
[86] Y. Hu, L. Wan, Y. Xiao, Y. Wang, Z. Wu, W. Guo, H. Yang, T. Hu, Enhanced reparative dentinogenesis of biphasic calcium phosphate ceramics containing calcium-deficient hydroxyapatite (CDHA) and strontium-incorporated CDHA in direct pulp capping, Mater, Today Commun 33 (2022) 104231, https://doi.org/10.1016/j.mtcomm.2022.104231.
[87] Y.M. Pupo, L.M.B. Leite, A.C. Senegaglia, L. Antunes, J.M. Nadal, E.L. De Lara, R. E. Saito, S.R.M. Antunes, W.F. Lacerda, P.V. Farago, Effect of hydroxyapatite microspheres, amoxicillin-hydroxyapatite and collagen–hydroxyapatite composites on human dental pulp-derived mesenchymal stem cells, Materials 14 (2021) 7515, https://doi.org/10.3390/ma14247515.
[88] C. Liang, L. Liao, W. Tian, Stem cell-based dental pulp regeneration: insights from signaling pathways, Stem Cell Rev. Rep. 17 (2021) 1251–1263, https://doi.org/10.1007/s12015-020-10117-3.
[89] Z. Xie, Z. Shen, P. Zhan, J. Yang, Q. Huang, S. Huang, L. Chen, Z. Lin, Functional dental pulp regeneration: basic research and clinical translation, Int. J. Mol. Sci. 22 (2021) 8991, https://doi.org/10.3390/ijms22168991.
[90] P. Kulan, O. Karabiyik, G.T. Kose, B. Kargul, The effect of accelerated mineral trioxide aggregate on odontoblastic differentiation in dental pulp stem cell niches, Int. Endod. J. 51 (2018) 758–766, https://doi.org/10.1111/iej.12747.
[91] S. Nam, J.-E. Won, C.-H. Kim, H.-W. Kim, Odontogenic differentiation of human dental pulp stem cells stimulated by the calcium phosphate porous granules, J. Tissue Eng. 2011 (2011) 812547, https://doi.org/10.4061/2011/812547.
[92] S. An, Y. Gao, J. Ling, X. Wei, Y. Xiao, Calcium ions promote osteogenic differentiation and mineralization of human dental pulp cells: implications for pulp capping materials, J. Mater. Sci. Mater. Med. 23 (2012) 789–795, https://doi.org/10.1007/s10856-011-4531-0.
[93] K. Huang, J. Wu, Z. Gu, Black phosphorus hydrogel scaffolds enhance bone regeneration via a sustained supply of calcium-free phosphorus, ACS Appl. Mater. Interfaces 11 (2019) 2908–2916, https://doi.org/10.1021/acsami.8b21179.
[94] L.E. Ling, L. Feng, H. Liu, D. Wang, Z. Shi, J. Wang, W. Luo, Y. Lv, The effect of calcium phosphate composite scaffolds on the osteogenic differentiation of rabbit dental pulp stem cells, J. Biomed. Mater. Res. 103 (2015) 1732–1745, https://doi.org/10.1002/jbm.a.35303.
[95] N. Liu, M. Zhou, Q. Zhang, T. Zhang, T. Tian, Q. Ma, C. Xue, S. Lin, X. Cai, Stiffness regulates the proliferation and osteogenic/odontogenic differentiation of human dental pulp stem cells via the WNT signalling pathway, Cell Prolif. 51 (2018) e12435, https://doi.org/10.1111/cpr.12435.
[96] J. Wang, H. Ma, X. Jin, J. Hu, X. Liu, L. Ni, P.X. Ma, The effect of scaffold architecture on odontogenic differentiation of human dental pulp stem cells, Biomaterials 32 (2011) 7822–7830, https://doi.org/10.1016/j.biomaterials.2011.04.034.
[97] X. Wei, J. Ling, L. Wu, L. Liu, Y. Xiao, Expression of mineralization markers in dental pulp cells, J. Endod. 33 (2007) 703–708, https://doi.org/10.1016/j.joen.2007.02.009.
[98] N. Luo, Y. Deng, J. Wen, X. Xu, R. Jiang, J. Zhan, Y. Zhang, B. Lu, F. Chen, X. Chen, Wnt3a-loaded hydroxyapatite nanowire@mesoporous silica core-shell nanocomposite promotes the regeneration of dentin-pulp complex via angiogenesis, oxidative stress resistance, and odontogenic induction of stem cells, Adv. Healthcare Mater. 12 (2023) 2300229, https://doi.org/10.1002/adhm.202300229.
[99] A. Simón-Soro, A. Mira, Solving the etiology of dental caries, Trends Microbiol. 23 (2015) 76–82, https://doi.org/10.1016/j.tim.2014.10.010.
[100] M.E. Khalaf, M. Karched, N.A. Shawaf, M.A. Qudeimat, In vitro investigation of the impact of contemporary restorative materials on cariogenic bacteria counts and gene expression, J. Dent. 133 (2023) 104486, https://doi.org/10.1016/j.jdent.2023.104486.
[101] Y. Zeng, Y. Chen, C. Duan, X. Jiang, Y. Wang, L. Zhang, A transcriptional analysis showing the effects of GH12 combined with fluoride for suppressing the acidogenicity of streptococcus mutans biofilms, Microorganisms 11 (2023) 1796, https://doi.org/10.3390/microorganisms11071796.
[102] S. Kulshrestha, S. Khan, S. Hasan, M.E. Khan, L. Misba, A.U. Khan, Calcium fluoride nanoparticles induced suppression of Streptococcus mutans biofilm: an in vitro and in vivo approach, Appl. Microbiol. Biotechnol. 100 (2016) 1901–1914, https://doi.org/10.1007/s00253-015-7154-4.
[103] I. Nedeljkovic, J. De Munck, V. Slomka, B. Van Meerbeek, W. Teughels, K.L. Van Landuyt, Lack of buffering by composites promotes shift to more cariogenic bacteria, J. Dent. Res. 95 (2016) 875–881, https://doi.org/10.1177/0022034516647677.
[104] F. Aykent, I. Yondem, A.G. Ozyesil, S.K. Gunal, M.C. Avunduk, S. Ozkan, Effect of different finishing techniques for restorative materials on surface roughness and bacterial adhesion, J. Prosthet. Dent 103 (2010) 221–227, https://doi.org/10.1016/S0022-3913(10)60034-0.